Introduction: Role of numerical experiments

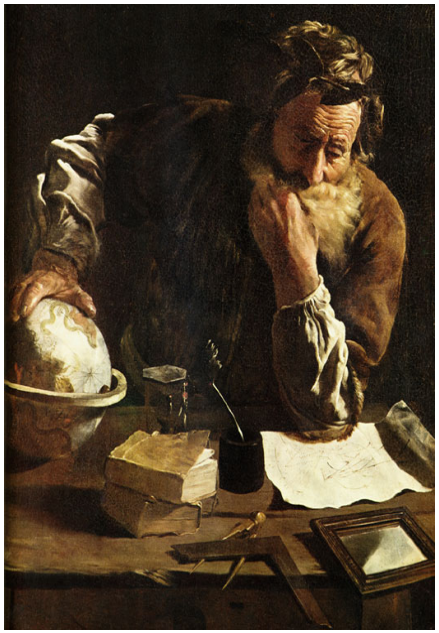

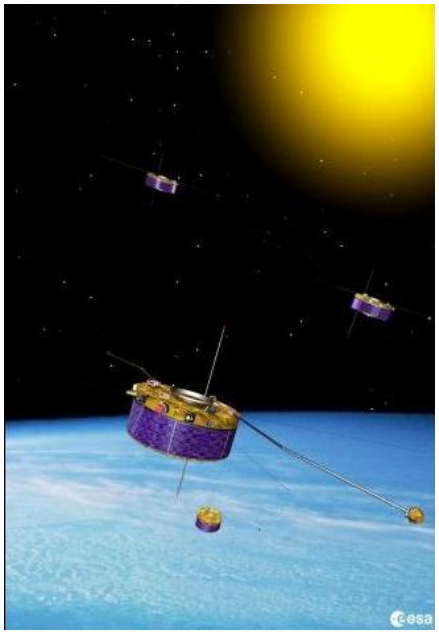

Maxwell equations

$$\frac{\partial \mathbf{B}}{\partial t} = -\nabla \times \mathbf{E},$$
$$\frac{1}{c^2}\frac{\partial \mathbf{E}}{\partial t} = \nabla \times \mathbf{B} - \mu_0 \mathbf{j},$$
$$\nabla \cdot \mathbf{B} = 0, \quad \nabla \cdot \mathbf{E} = \varrho/\varepsilon_0.$$

Vlasov equations

$$\frac{\partial f_e}{\partial t} + \mathbf{v}_e \cdot \frac{\partial f_e}{\partial \mathbf{x}} - \frac{e}{m_e}(\mathbf{E} + \mathbf{v}_e \times \mathbf{B}) \cdot \frac{\partial f_e}{\partial \mathbf{v}_e} = 0,$$
$$\frac{\partial f_p}{\partial t} + \mathbf{v}_p \cdot \frac{\partial f_p}{\partial \mathbf{x}} + \frac{e}{m_p}(\mathbf{E} + \mathbf{v}_p \times \mathbf{B}) \cdot \frac{\partial f_p}{\partial \mathbf{v}_p} = 0,$$

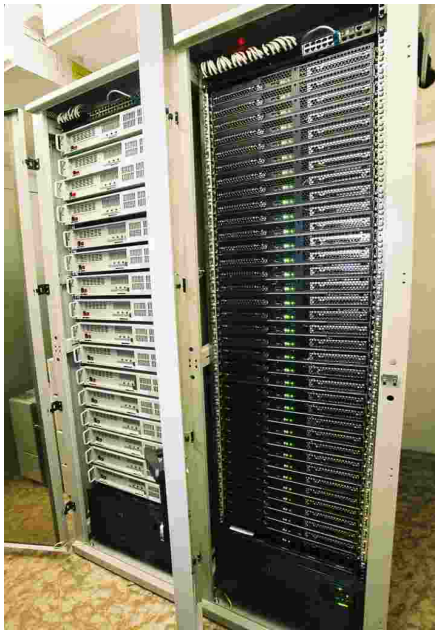

- Humans try to explain events ongoing in the surrounding nature since early days. Over centuries: experiment and theory.
- Technological advances: today we use spacecraft measurements to improve our knowledge about processes ongoing in space environment. On their basis we built up our theoretical models.
- Advances in computer technology achieved in last decades allow us to use theoretical knowledge to formulate studied problems in the form of numerical models. Extension of our theoretical/experimental capabilities.

Introduction: Simulations vs. in situ experiments

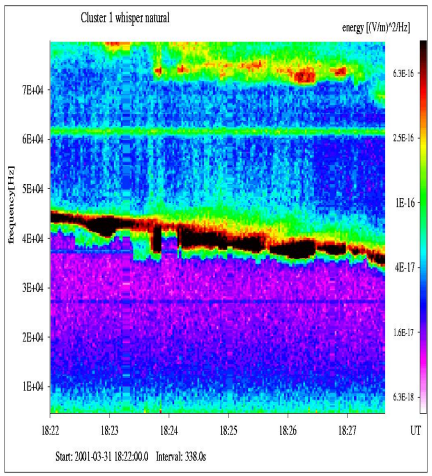

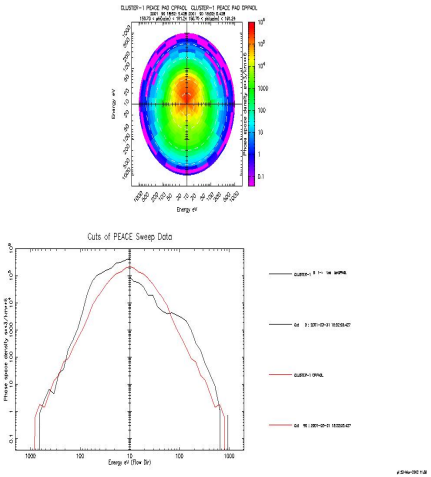

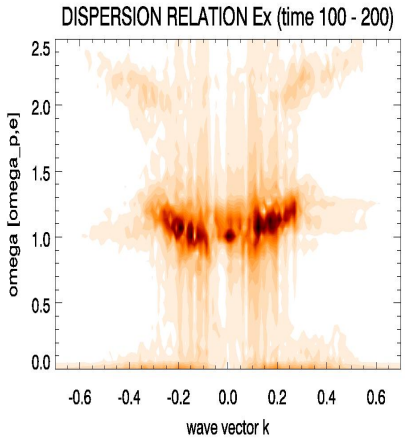

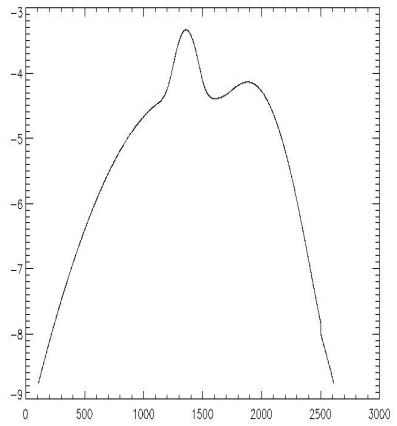

- LEFT: data acquired by the electron spectrometer PEACE and by a wave analyzer WHISPER onboard Cluster II spacecraft: waves generated in a space plasma at fundamental frequency and twice the plasma frequency.
- RIGHT: analogical data from a numerical experiment. We use a model of electron VDF with an electron beam. We can observe corresponding wave emissions in a numerical model.
- The spacecraft must be present at the place of the interesting event.
  In the case of the numerical simulation we can change different input parameters of our model and then observe, when the given phenomena reaches its maximum, or when the process is not ongoing at all.

Numerical model: Dimensionless simulation units

Physics is essentially dimensionless (important are relative rather than absolute values), it scales with dimensions typical for the given problem. In a numerical we use:

- $q = 1, m_p = 1.$
- We use proton inertial length in the solar wind $\Lambda_{p\mathrm{sw}} = c/\omega_{p\mathrm{sw}}$ and the inverse of the proton cyclotron frequency $\Omega_{p\mathrm{sw}}^{-1}$ as spatial and temporal units respectively.
- i.e. $n_{p\mathrm{sw}} = 1, \mathbf{B}_{0\mathrm{sw}} = 1, v_{A\mathrm{sw}} = 1.$
- Hermean radius (for example) in the units of the numerical model varies with the value of $\Lambda_{p\mathrm{sw}}$ in SI units.
- **Consequently: In generall - typical spatio temporal sizes of the studied interaction between a stellar flow and a moon or planet depend naturally on the physical properties of the flow (its density and magnetic field in it)**

Planets of our Solar system

Name	distance	n_{pSW}	B_{SW}	Λ_{iSW}	v_{ASW}	radius R		$v_{sw} = 300km/s$	dipole moment M	
	[AU]	[cm^{-3}]	[nT]	[km]	[km s^{-1}]	[km]	[Λ_i]	[v_A]	[M_{Earth}]	[$\Lambda_i^3\ B_{sw}/\mu_0$]
Mercury	0.31	73	46	26.7	118	2 439	**91**	**2.5**	$4.7 \cdot 10^{-4}$	**$5.4 \cdot 10^{7}$**
	0.47	32	21	40	82	2 439	**60**	**3.6**	$4.7 \cdot 10^{-4}$	**$3.5 \cdot 10^{7}$**
Venus	0.72	14	10	61	59	6 052	**99**	**5**	-	-
Earth	1.0	7	6	86	50	6 378	**74**	**6**	1.0	**$2.6 \cdot 10^{9}$**
Mars	1.5	3.1	3.4	129	42	3 397	**26**	**7**	-	-
Jupiter	5.2	0.26	0.83	447	36	71 398	**160**	**8**	20.000	**$2.7 \cdot 10^{13}$**
Saturn	9.6	0.076	0.44	827	35	60 000	**73**	**9**	540	**$2.16 \cdot 10^{11}$**
Uranus	19.1	0.019	0.22	1 654	35	25 400	**15**	**9**	48	**$4.8 \cdot 10^{9}$**
Neptune	30.2	0.0077	0.14	2 599	35	24 300	**9**	**9**	26	**$1.0 \cdot 10^{9}$**
Pluto	39.4				35	2 500		**9**	unknown	unknown

- The Earth magnetic dipole moment is $M_{\text{Earth}} = 8 \cdot 10^{22}\ Am^2$.
- Mercury is the most likely (magnetized) candidate to be studied by a global kinetic numerical model beside unmagnetized planets Venus and Mars
- Effect of denser stellar flow at Mercury: from physical point of view the size of Mercury is comparable to Earth
- Mercury also changes its diameter in the stellar flow of given desity thanks to its eccentric Solar orbit
- Pluto almost can not be simulated by a hybrid code and its study requires a full particle in cell code

Numerical codes

- Magnetohydrodynamic (MHD) codes: traditional codes used for global simulations of the interaction betwee stellar flows and moons and planets
  - Alow 3D modeling on global scales
  - Neglect kinetic effects and hence wave-particle interactions
- Particle in cell (PIC): use macro-particles to describe both electrons and ions
  - Include (all) kinetics for both electrons and ions
  - Require to use unrealistic parameters (for example, mass ratio)
- A compromise: Hybrid model [Alan Matthews, 1994]: treat electrons as fluid
  - Include ion kinetics
  - Allow ”realistic” parameters on a global scale
  - Do not include electron kinetics, some types of waves, if excited, can not interact with electrons and should be artificially dumped.

Hybrid Expanding Box code: The motivation

- Properties of collisionless plasmas are largely determined by wave-particle interactions
- A homogeneous slowly expanding plasma (without any fluctuating wave energy evolves adiabatically. The ion parallel and perpendicular temperatures $T_{\parallel}$ and $T_{\perp}$ satisfy the CGL equations $T_{\parallel} \propto B$ and $T_{\perp} \propto n^2/B^2$, respectively
- In the case of a strictly radial expansion, $\boldsymbol{B}(0) = (1,0,0)$, the temperature anisotropy evolves as $T_{\perp}/T_{\parallel} \propto (1+t/t_e)^{-2}$, where $t_e = R_0/U$ is the characteristic time of the expansion (R_0 is initial distance from the Sun, U is the (constant) solar wind speed
- In slowly expanding (or compressed) plasma temperature anisotropies naturally develop. Temperature anisotropy (i.e. departure from Maxwellian particle distribution function) represent a possible source of free energy for many different instabilities.
- As a feed-back, the instabilities constrain the shape of particle distribution functions.

Solar wind plasma: Protons

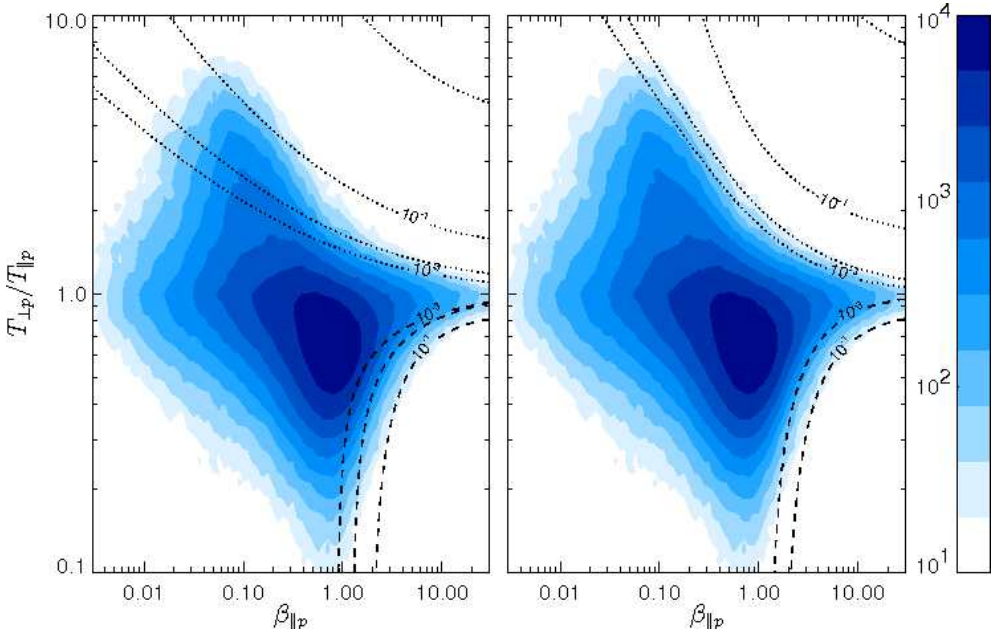

[Hellinger et al., 2006]

- Both panels show a color scale plot of the relative frequency of $(\beta_{p\parallel}, T_{p\perp}/T_{p\parallel})$ in the WIND/SWE data (1995-2001) for the solar wind $v_{\mathrm{SW}} < 600$ km/s
- The over plotted curves show the contours of the maximum growth rate (in units ω_{cp}) in the corresponding bi-Maxwellian plasma
  - proton cyclotron instability (solid curves)
  - parallel fire hose instability (dashed curves)
  - proton mirror instability (dotted curves)
  - oblique fire hose instability (dash-dotted curves)

Solar wind plasma: Electrons

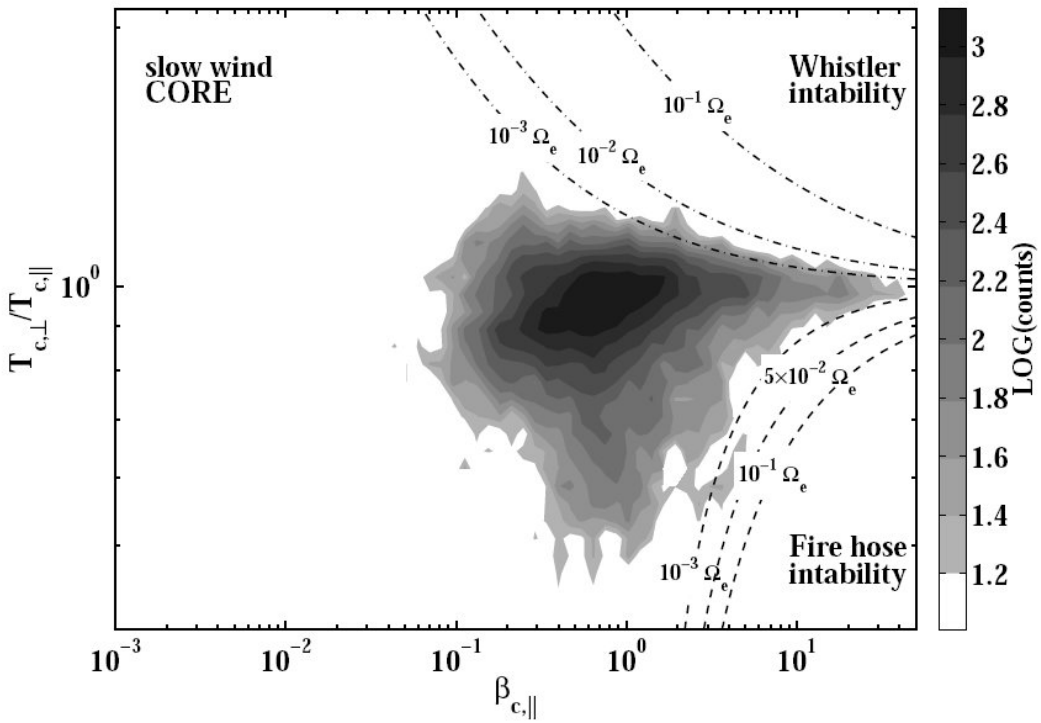

[Stverak et al., 2008]

- Panel shows a gray shaded scale plot of the relative frequency of $(\beta_{p\parallel}, T_{p\perp}/T_{p\parallel})$ in the Helios data for the solar wind $v_{SW} < 600$ km/s
- The over plotted curves show the contours of the maximum growth rate (in units ω_{ce}) in the corresponding bi-Maxwellian plasma
  - whistler instability (dash-dotted curves)
  - parallel electron fire hose instability (dashed curves)

Hybrid Expanding Box code: The design

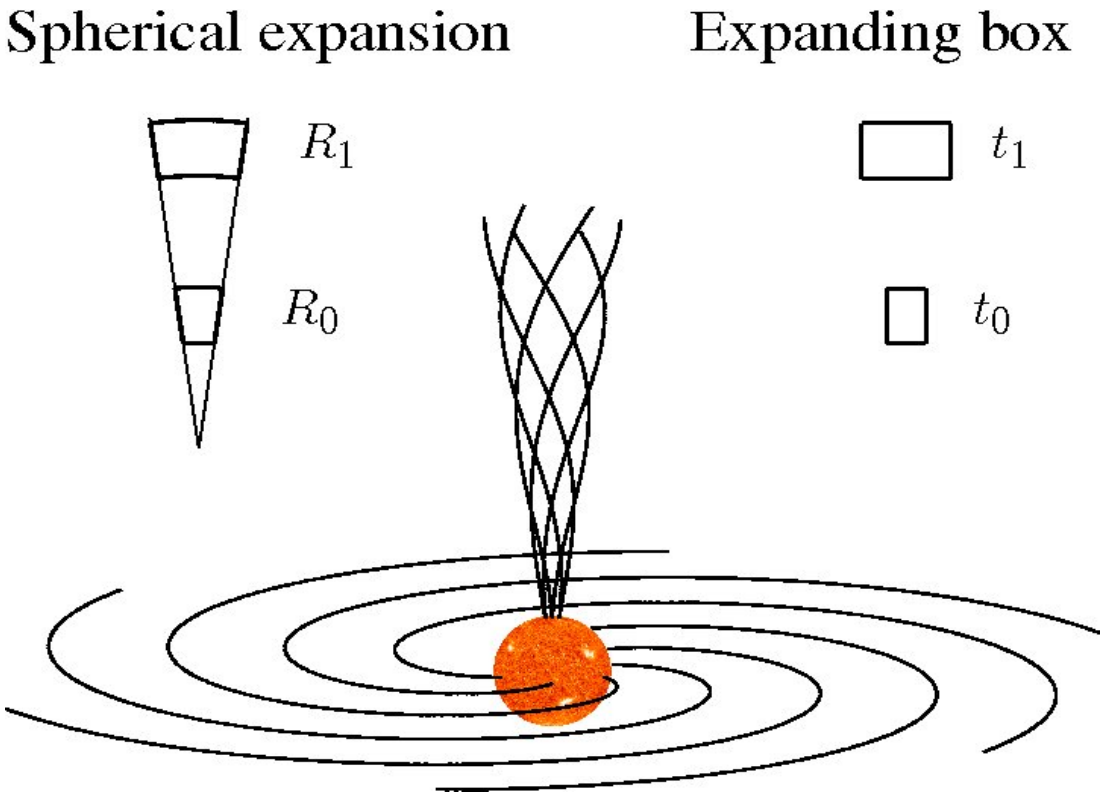

- The stellar plasma flow is subject to the continuous radial expansion. It can be also subject of compression (in a planetary magnetosheath) and/or torsion caused by a velocity shear
- HEB code uses Vlasov equations in such a way that we can study a given volume of continuously expanding plasma in a simulation box (1D or 2D) with periodic boundary conditions

Magnetosheath plasma stretching

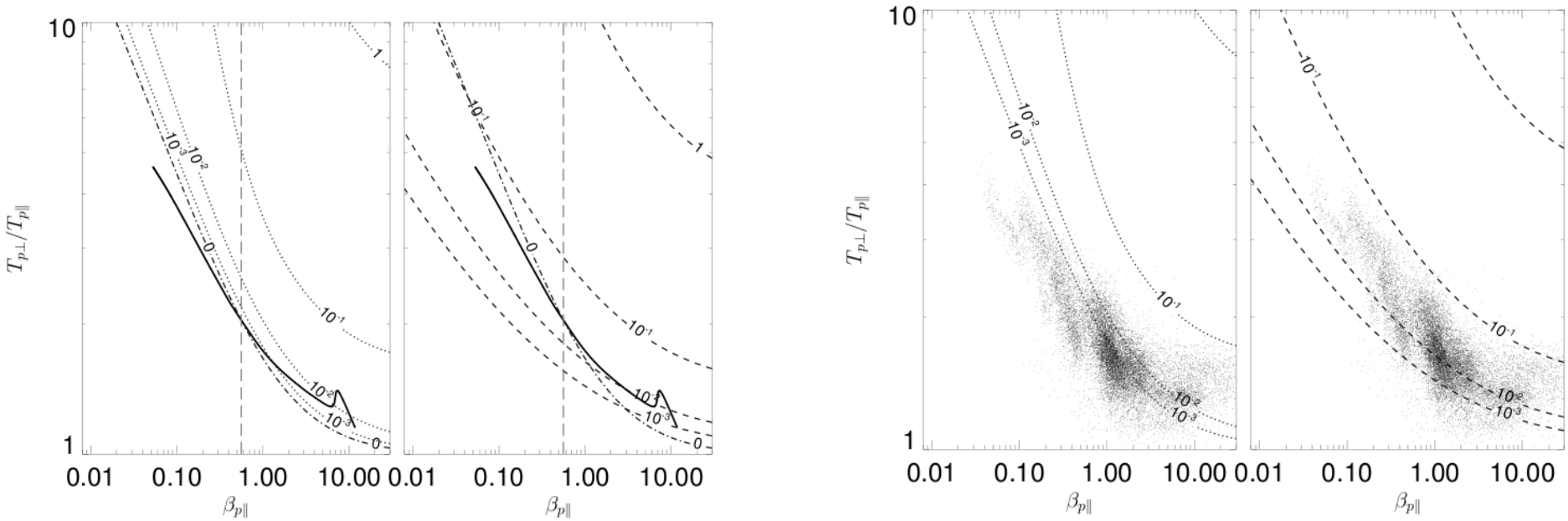

- LEFT: Evolution during the numerical simulation of plasma stretching in the space $(\beta_{\parallel}, T_{p\perp}/T_{p\parallel})$. The evolution (solid line) follows initially the adiabatic prediction. The over plotted curves show the contours of the maximum growth rate (in units of ω_{cp}) (left) for the proton cyclotron instability and (right) the mirror proton instability.
- RIGHT: In situ observations made by HIA experiment
- [Travnicek et al., 2007]

Magnetosheath plasma stretching

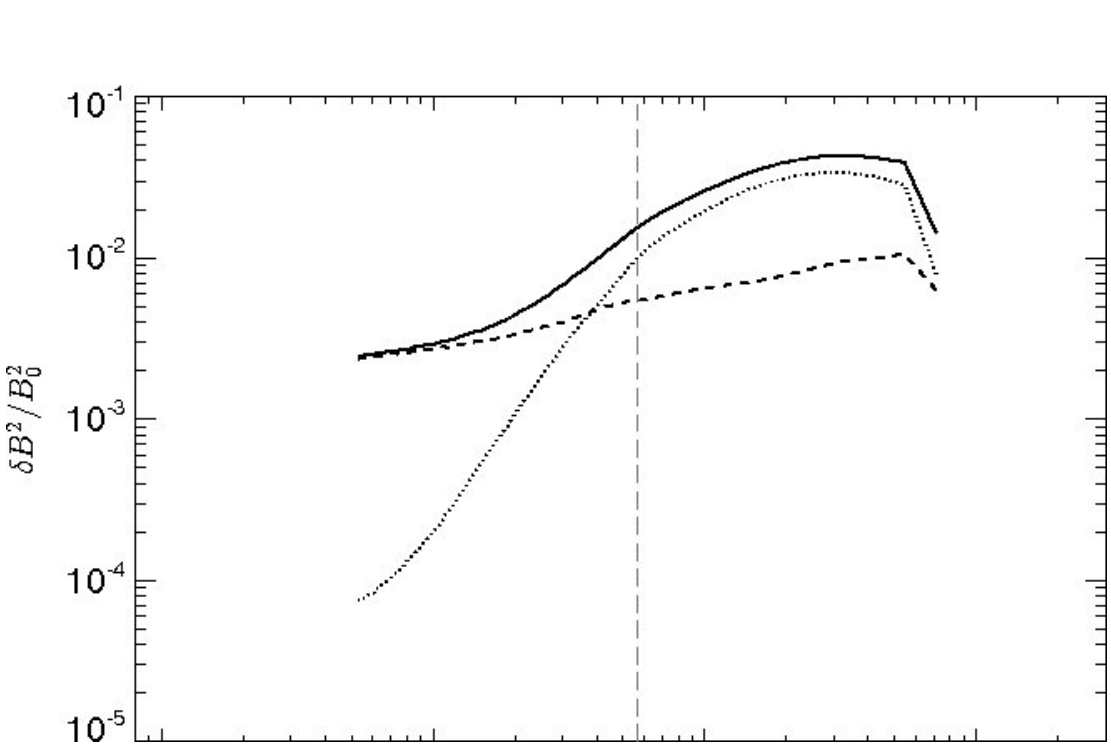

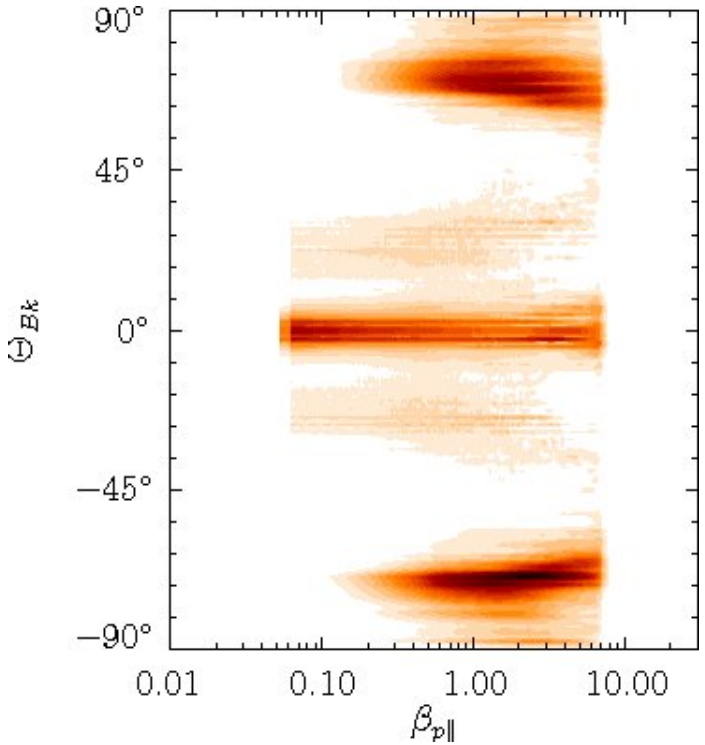

LEFT: The panel shows the total fluctuating magnetic energy $\delta B^2/B_0^2$ (solid curve) as a function of $\beta_{p\parallel}$. The dotted curve corresponds to the mirror fluctuating magnetic energy $\delta B^2_{\rm mir}/B_0^2$ whereas the dashed curve corresponds to the proton cyclotron fluctuating magnetic energy $\delta B^2_{\rm PC}/B_0^2$. RIGHT: The panel shows a coloured plot of the fluctuating magnetic energy $\delta B^2/B_0^2$ as a function of $\beta_{p\parallel}$ and $\Theta_{\boldsymbol{kB}}$. The gray dashed vertical line denotes $\beta_{p\parallel}$ for which the simulation reaches the linear mirror threshold.

Interaction of Enceladus's Water Plume with Saturnian Magnetosphere via Hybrid Numerical Simulations

Pavel M. Trávníček[1,2], Štěpán Štverák [2], Krishan K. Khurana [3], Petr Hellinger [2], Michele K. Dougherty [4], Jan Somr

[1]Astronomical Institute, ASCR, Prague, Czech Republic

[2]Institute of Atmospheric Physics, ASCR, Prague, Czech Republic [3]Institute of Geophysics and Planetary Physics, UCLA, Los Angeles, US [4]Space and Atmospheric Physics Group, Imperial College, London, UK

AGU San Francisco, December 16, 2008

Abstract

Several close Cassini flybys of the Santurnian moon Enceladus provided direct in situ measurements of neutral water molecules escaping from the surface showing their interaction with the ambient plasma environment. Cassini measurements indicate Enceladus to act as an obstacle to the magnetized Saturnian plasma flow resulting in an effect of field line draping. Ionization of escaping neutrals by way of charge exchange with the ambient plasma produces fresh ions which are picked up by the Saturnian magnetosphere. The Saturnian co-rotating plasma flow therefore slows down and the ambient magnetic field is affected. We study these local plasma interaction of Enceladus and its neutral water plume with the Saturnian magnetosphere by using a full 3D hybrid code numerical simulation. The results of our model are subsequently compared with Cassini observations. Since a complete and accurate description of Enceladus surroundings is still missing, the initialization of our simulations is based on currently published estimations. However, by use the hybrid code we are able to recover very similar magnetic field signatures as some of those really observed by Cassini spacecraft.

Cassini flybys

Previous (2005)

E3 2005-Feb-17
C/A 3:30

E4 2005-Mar-9
C/A 9:08

E11 2005-Jul-14
C/A 19:55

New (2008)

E61 2008-Mar-12
C/A 19:06

E80 2008-Aug-11
C/A 21:06

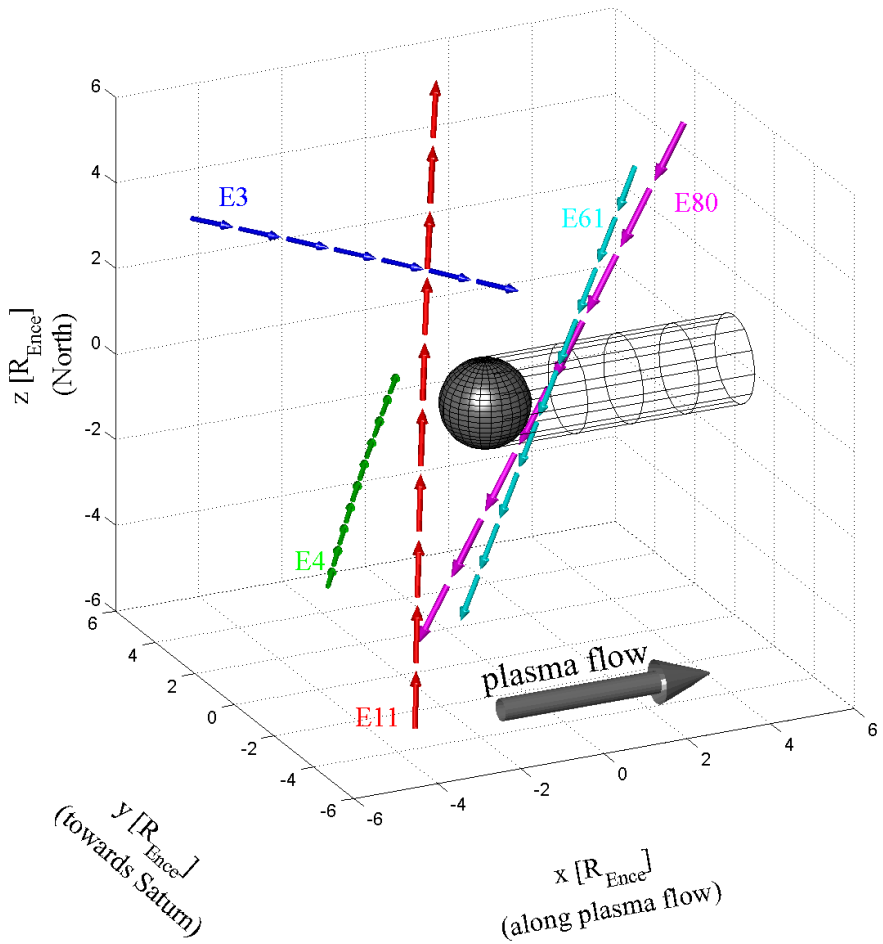

Magnetic field signatures (2005)

Observed magnetic field perturbations *[Dougherty et al. 2006]* seem to be consistent with an Alfvénic wing current system.

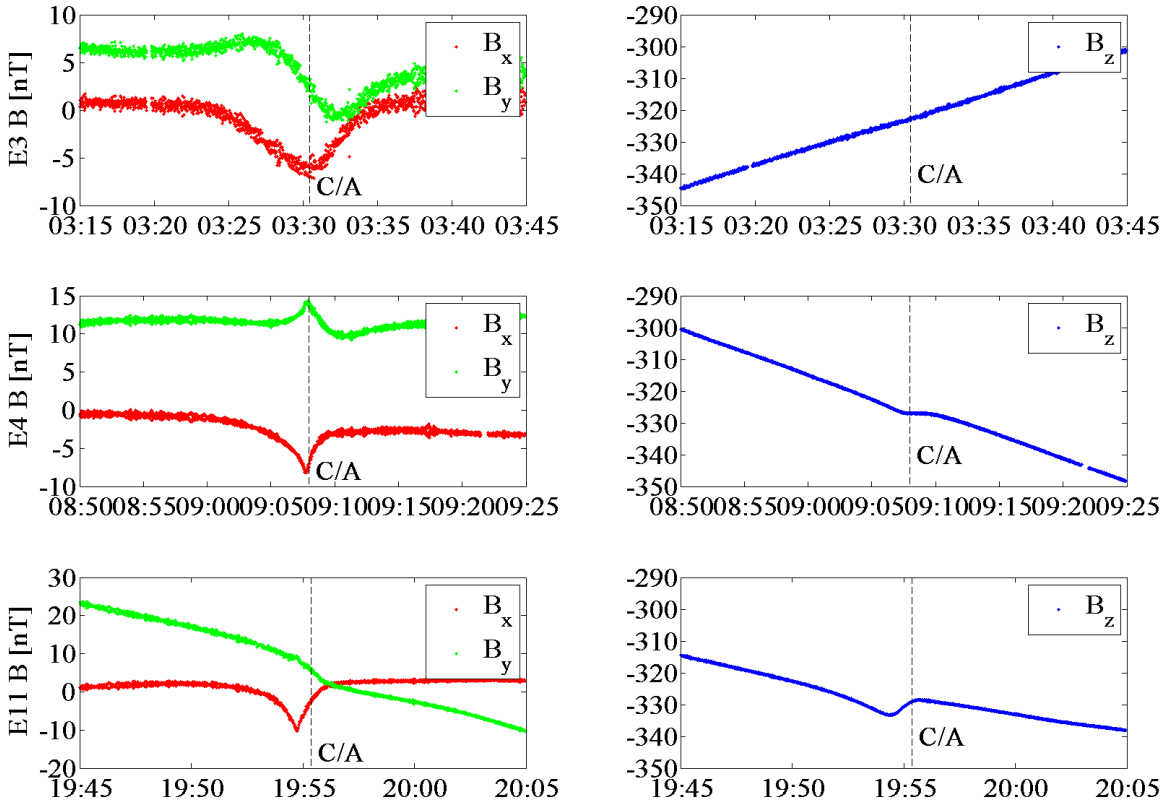

Magnetic field signatures (2008)

In 2008 the two flybys crossed the wake behind Enceladus very close ($< 2R_E$) to the moon's surface.

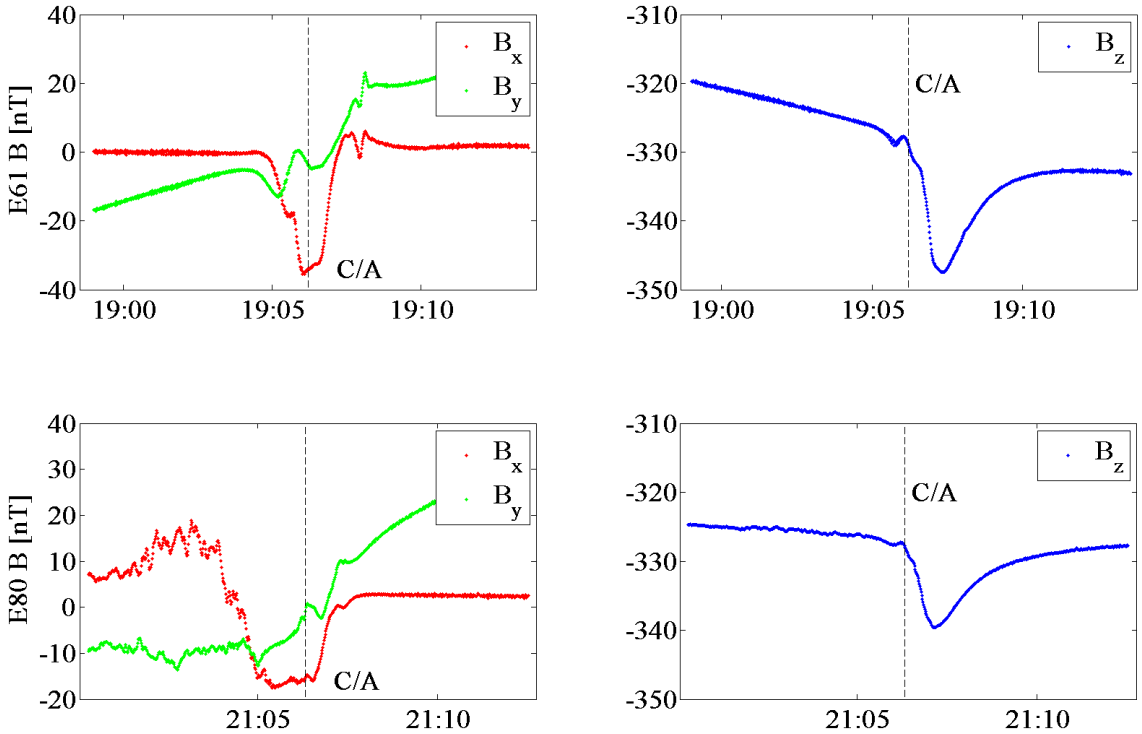

H_2O Distribution near Enceladus

Direct observations of water vapor were made by INMS and UVIS - flyby E11 (2005-Jul-14). Results suggest nonuniform source of water escaping from Enceladus - much stronger source near south pole.

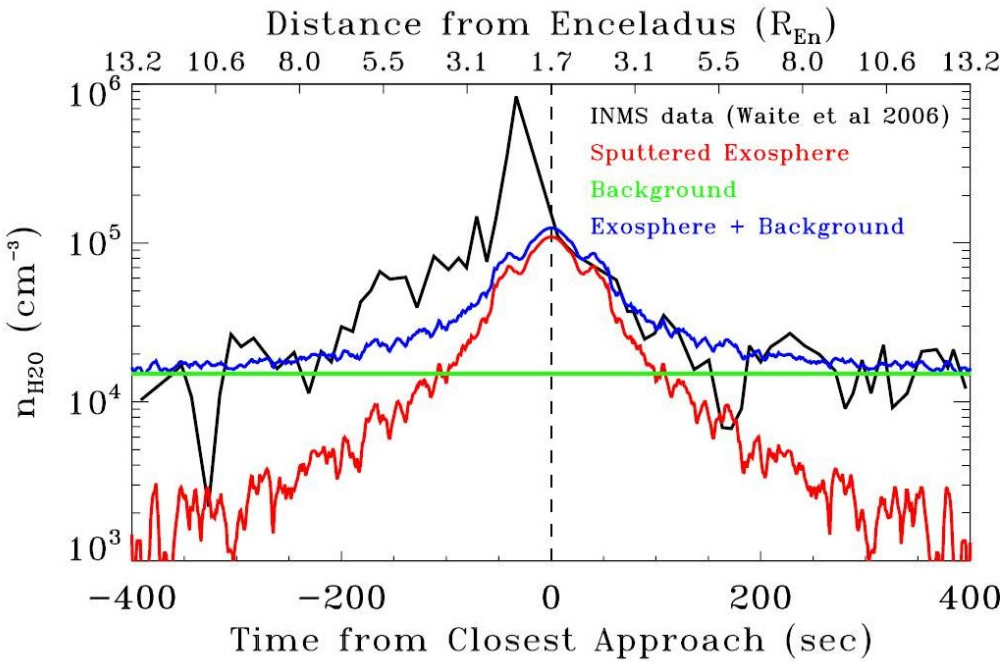

Exospheric model compared with direct in situ measurements *[Burger et al. 2007]*

Modeling H_2O Plume - MC simulation

We use a simplified Monte Carlo model to estimate the expected distribution of H_2O molecules near the south pole of Enceladus. A snapshot of this model is then used in the hybrid simulation as a stationary neutral background.

- super particles (SP) ejected from south of $-83.5°$
- uniform distribution per source surface
- Gaussian distribution of ejection velocity
- collisions and gravity not concerned

Setup

Parameter	Units	Value
time step	s	1
source rate	SP/s	100
polar cap	degree	15
$\mu(v_{eject})$	m/s	500
$\sigma(v_{eject})$	m/s	200

Modeling H_2O Plume - MC Result

Estimation of the H_2O distribution around Enceladus including a theoretical exosphere and background. SP density of the water plume are transformed into real physical units by calibration to INMS measurements from flyby E11 (2005-Jul-14).

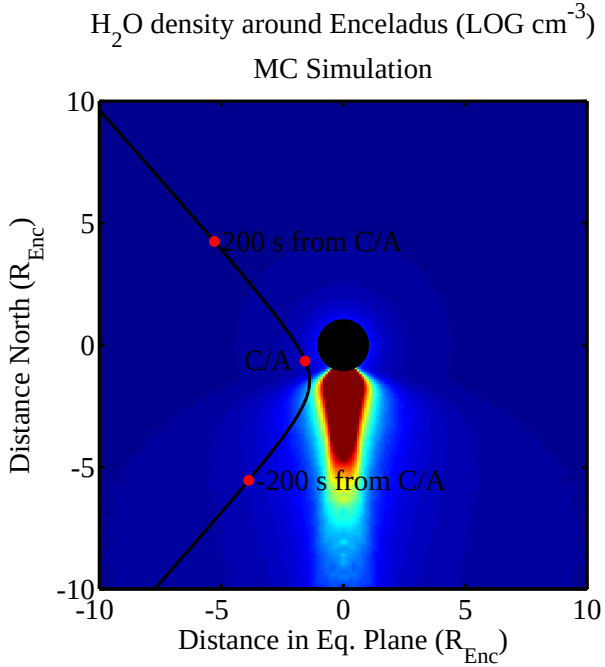

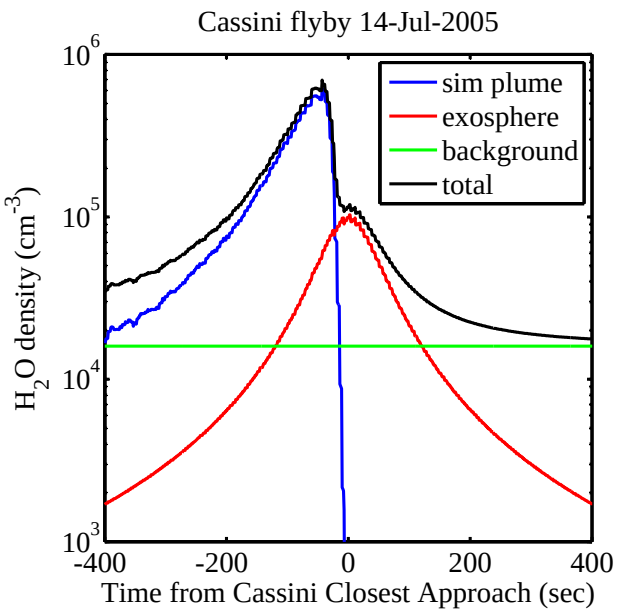

Modeling H_2O Plume - Analytic

For testing of different plume configurations and properties we use a parametric analytical model of an expanding generic ellipsoidal volume.

- $n(r) = n_0 \frac{l(r_0)}{l(r)}$
- $l(r) \approx \frac{\pi}{2}[(3/2(a+c) - \sqrt{ac}) + (3/2(b+c) - \sqrt{bc})]$

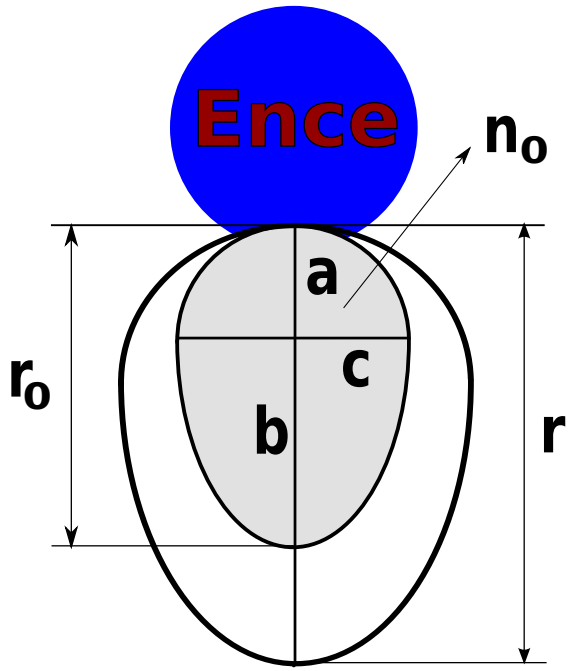

Mass loading process

In the Saturn magnetosphere the neutrals ejected from the surface of Enceladus are ionized. The newly created ions with velocities smaller compared to the ambient plasma then act as an obstacle to the magnetized plasma flow draping its field lines. Main source of the ionization process represent ion-neutral reactions:

Reaction	σ [Å]	
$H^+ + H_2O \rightarrow H + H_2O^+$	42	*Lindsay et al. 1997*
$O^+ + H_2O \rightarrow O + H_2O^+$	36	*Dress et al. 1996*
$H_2O^+ + H_2O \rightarrow H_2O + H_2O^+$	8.1	*Lishawa et al. 1997*
$H_2O^+ + H_2O \rightarrow OH + H_3O^+$	1.8	*Lishawa et al. 1997*
$OH^+ + H_2O \rightarrow OH + H_2O^+$	8.1	*Burger et al. 2007*

Table: Ion-neutral reaction and corresponding effective cross-section for ion-neutral relative velocity of 26 km/s.

Mass loading process - Rates

The total mass loading rate R_{tot} is computed by

$$R_{tot} = \sum_{j \in \{ion\ spec\}} \int_{imp.\ region} n_{H_2O} n_{ion,j} \sigma_j v_{rel,j} dV$$

where

- n_{H_2O} is H_2O neutrals density
- $n_{ion,j}$ is density of j^{th} ion species
- σ_j is effective cross-section
- $v_{rel,j}$ is ion-neutral relative velocity

The total mass load production is estimated in the interaction region between 1.5 and 3 kg/s *[Burger et al. 2007]*.

3D Hybrid Simulation - Initialization

Spatial resolution $\triangle x$, $\triangle y$, $\triangle z$	1.0 Λ_{p0}
Time step $\triangle t$	0.05 Ω_{p0}^{-1}
Radius of Enceladus	R_E = 8.57 Λ_{p0}
Box dimensions	in [R_E]
x	(-12.0,10.0)
y	(-12.5,12.5)
z	(-13.0,9.0)
Ion species (plasma flow)	H^+, H_2O^+, H_3O^+ N/A
relative density	10/90 %
Ion species (reactions)	H_2O^+, H_3O^+
β_e	0.001
$\beta_{H^+}, \beta_{H_2O^+}$	0.0002, 0.008
plasma flow velocity	0.04 v_A

3D Hybrid Simulation - Initialization MF, E 3, 4 and 11

Theoretical Saturnian dipole field ($B_0 = B_{eq}(r_0) = (0, 0, -1)$)

- $B_x = B_{x0}\frac{r_0^3}{r^5}zx$
- $B_y = B_{y0}\frac{r_0^3}{r^5}zy$
- $B_z = B_{z0}\frac{r_0^3}{r^5}(z^2 - 1/3r^2)$

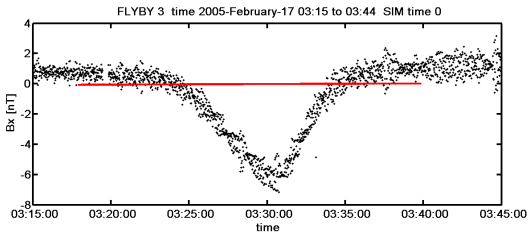

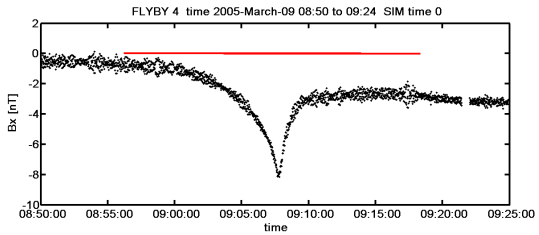

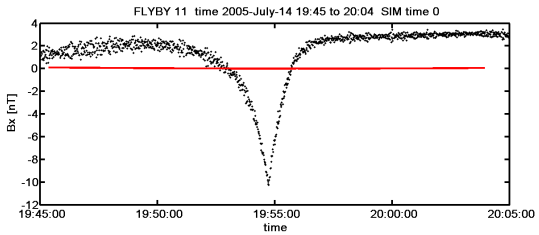

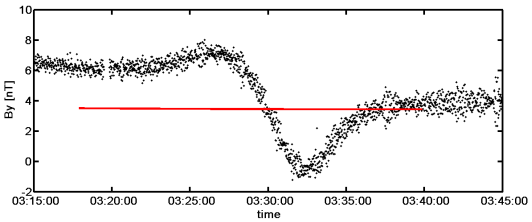

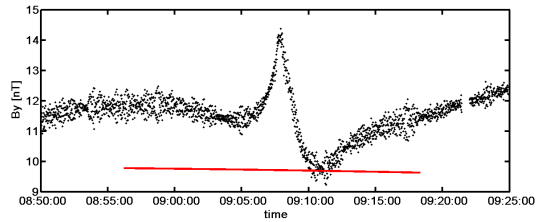

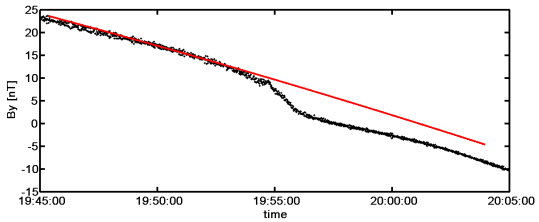

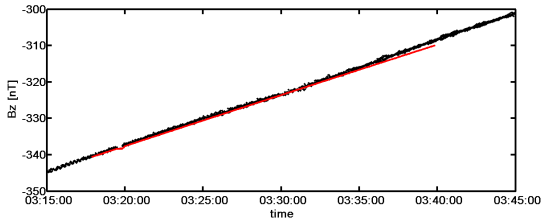

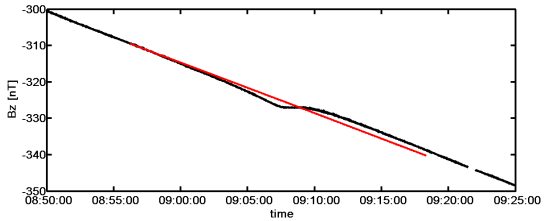

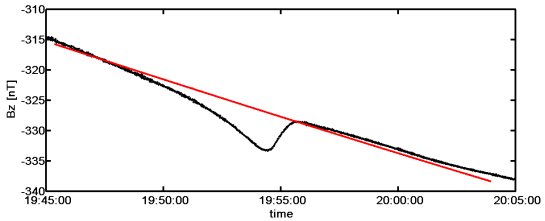

3D Hybrid Simulation - Initialization MF, E61 and E80

Virtual flybys for E61 and E80 at simulation time 0.

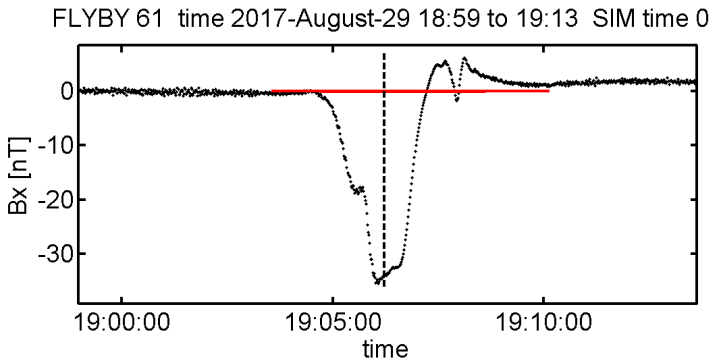

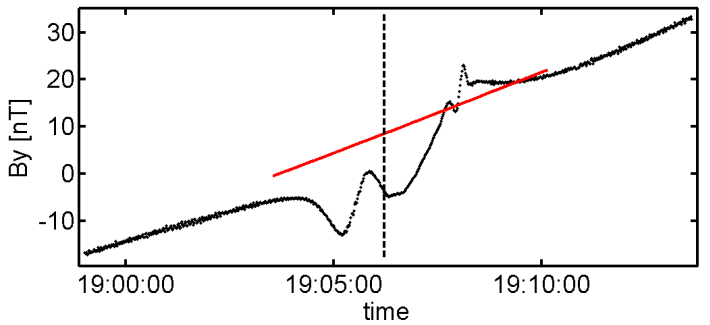

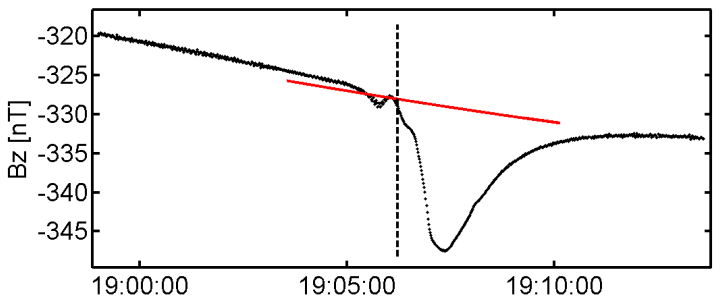

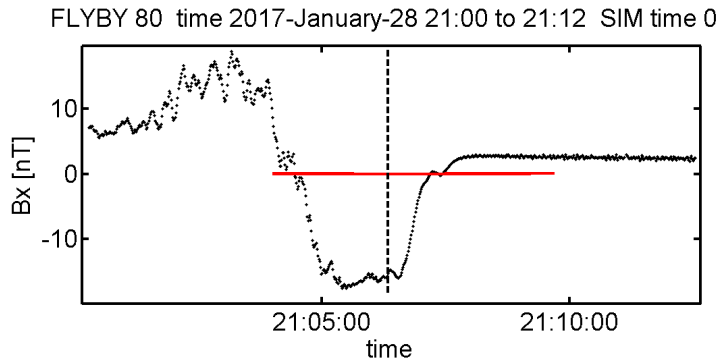

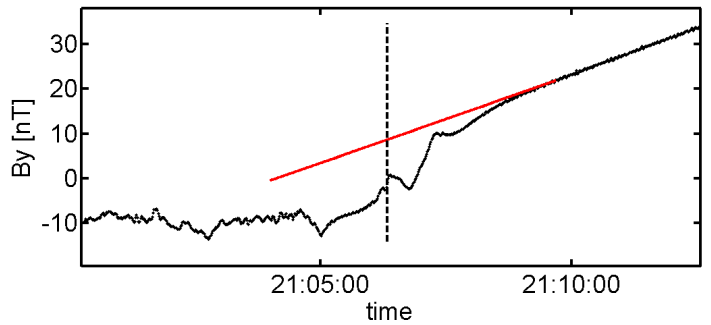

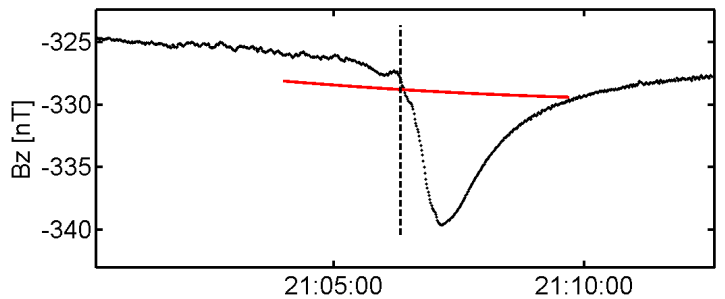

3D Hybrid Simulation Results - Ion densities t=600

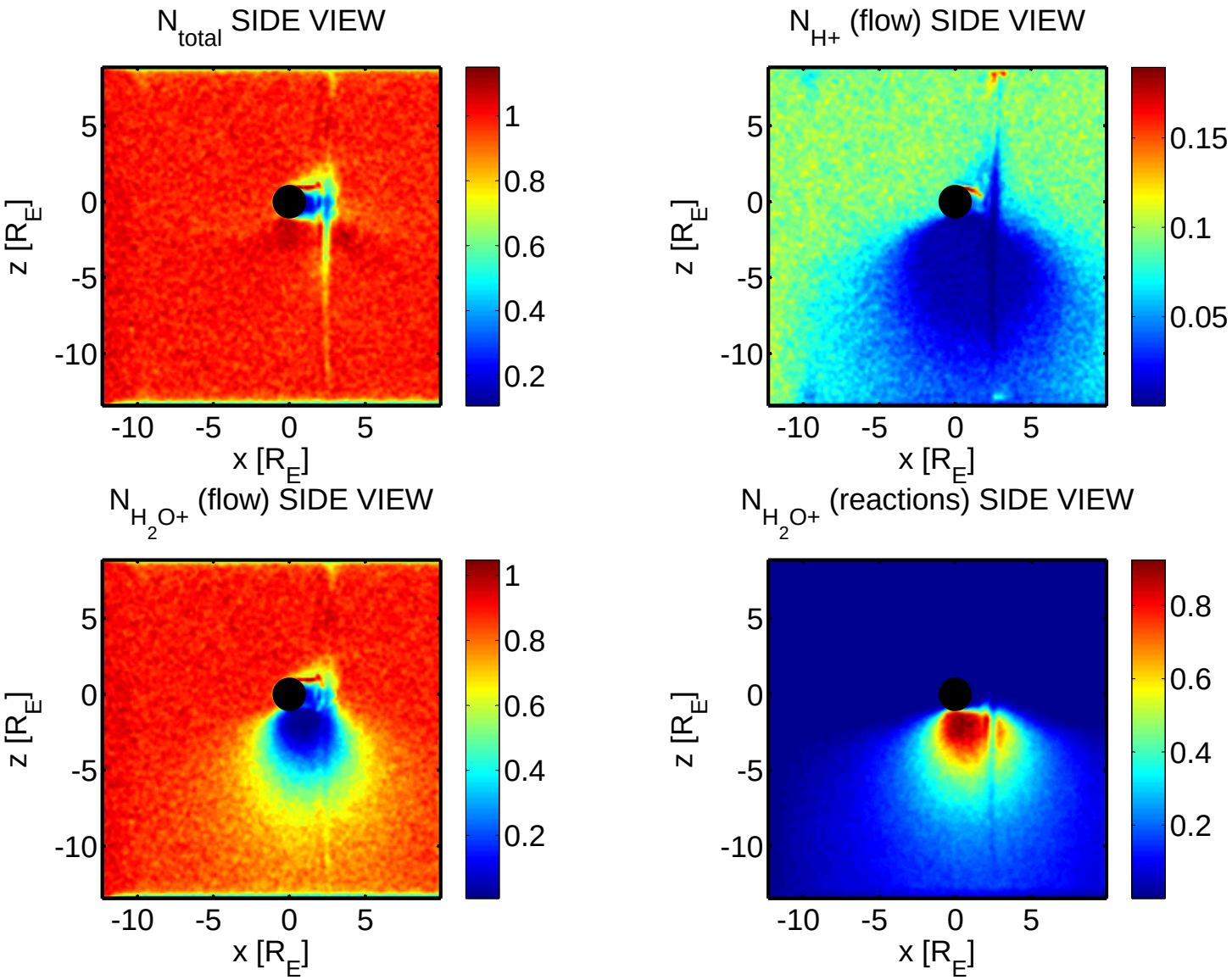

3D Hybrid Simulation Results - MF components

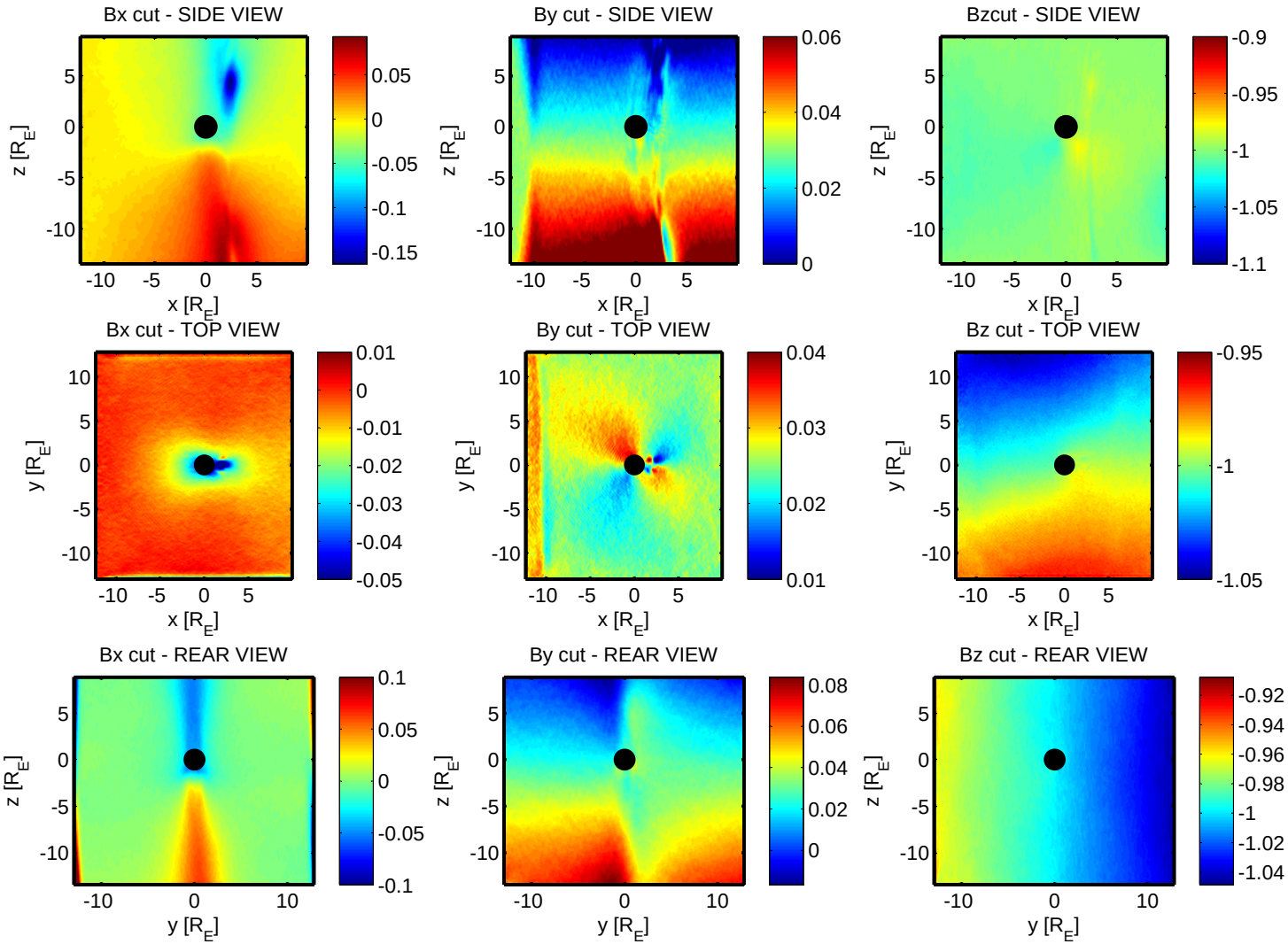

3D Hybrid Simulation Results - E 3

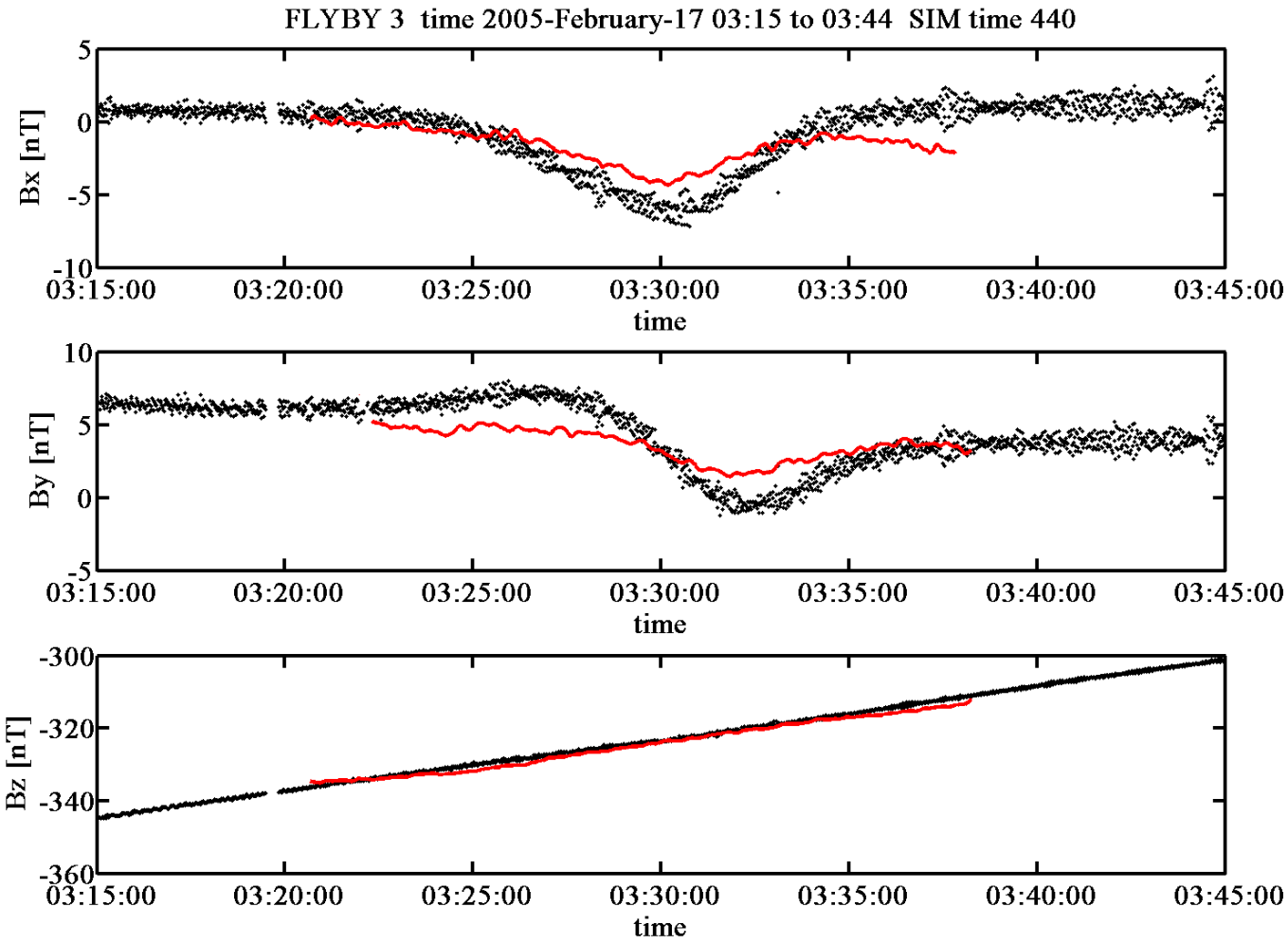

3D Hybrid Simulation Results - E 4

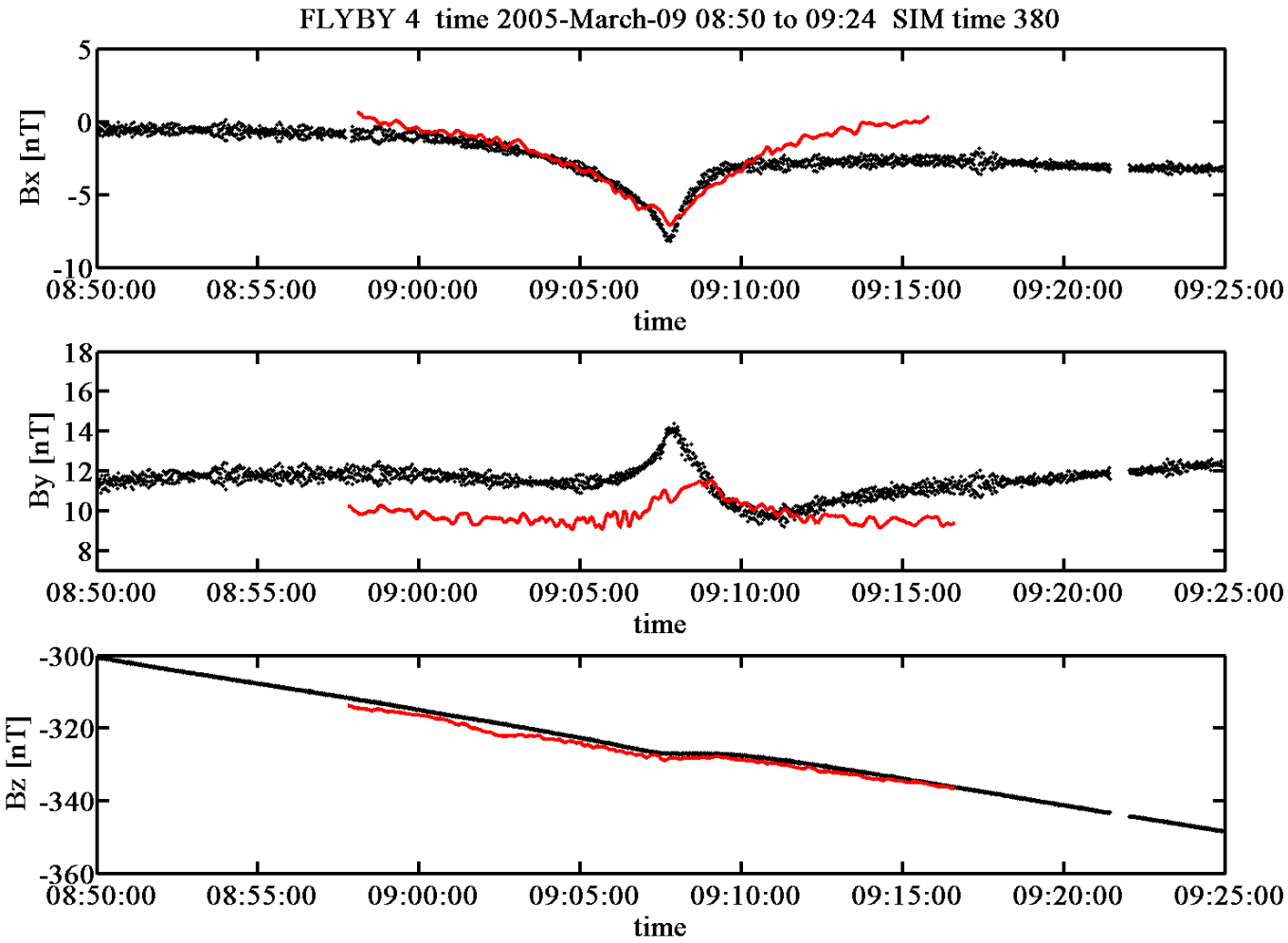

3D Hybrid Simulation Results - E 11

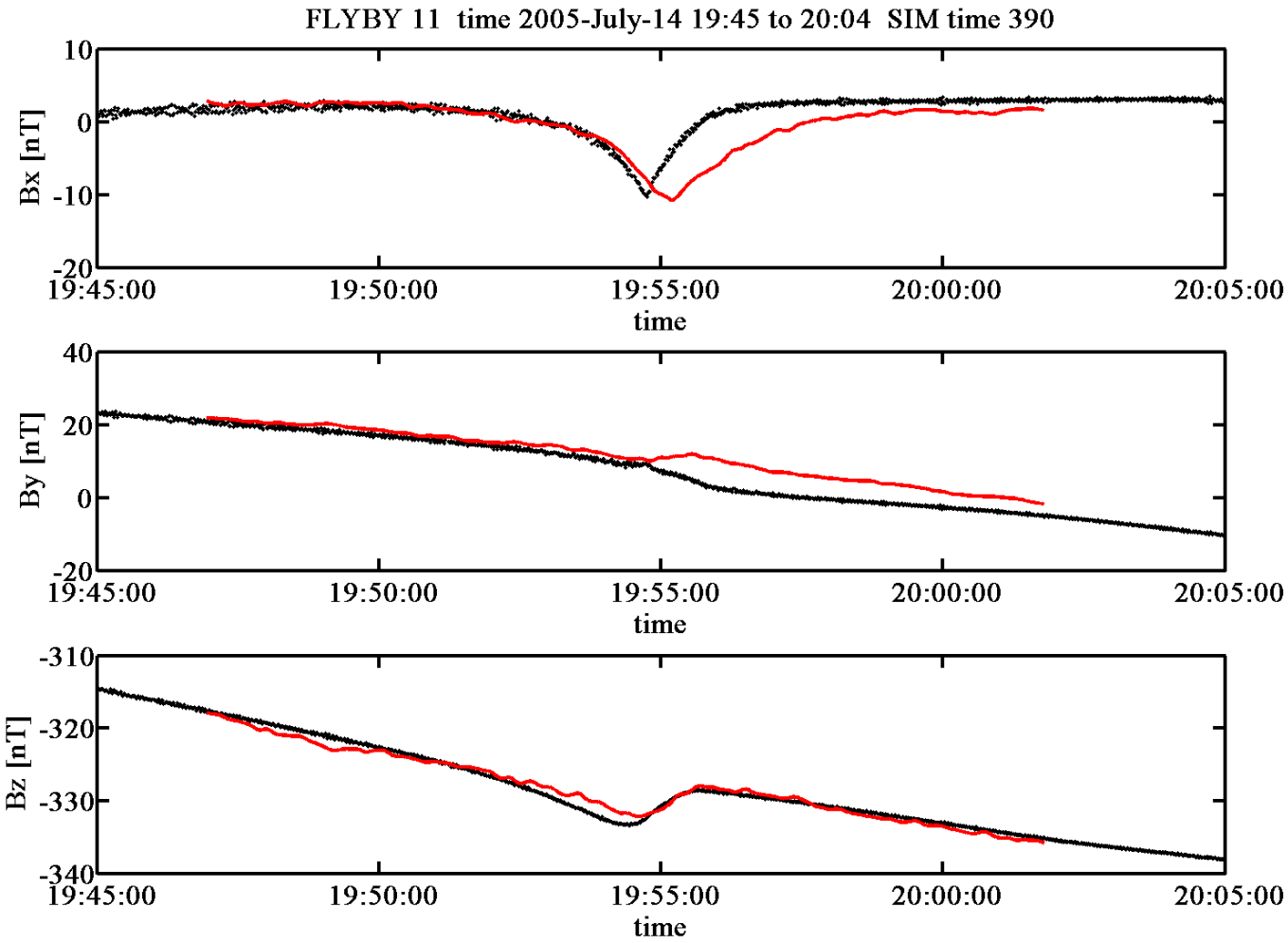

3D Hybrid Simulation Results - E 61

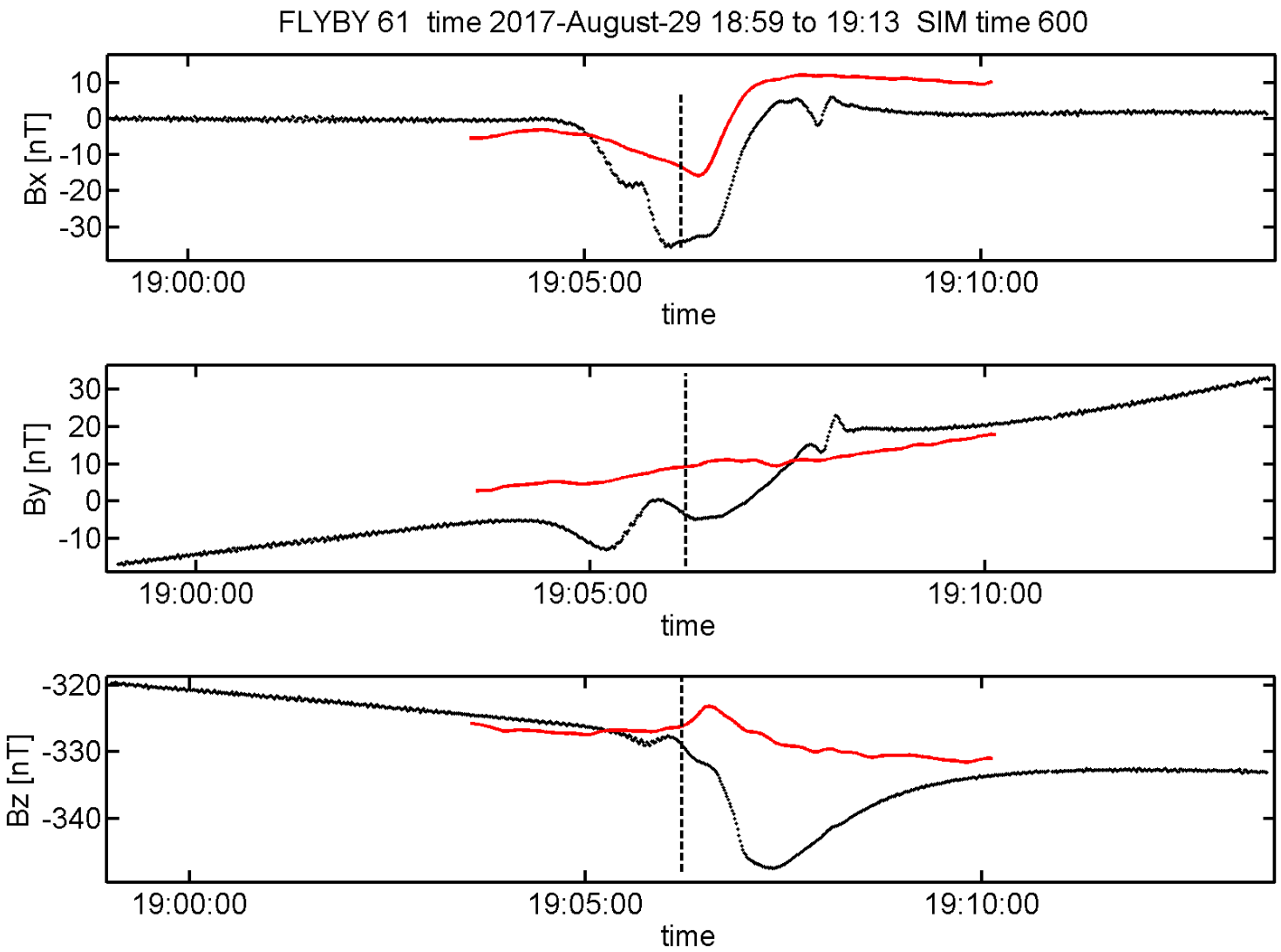

3D Hybrid Simulation Results - E 80

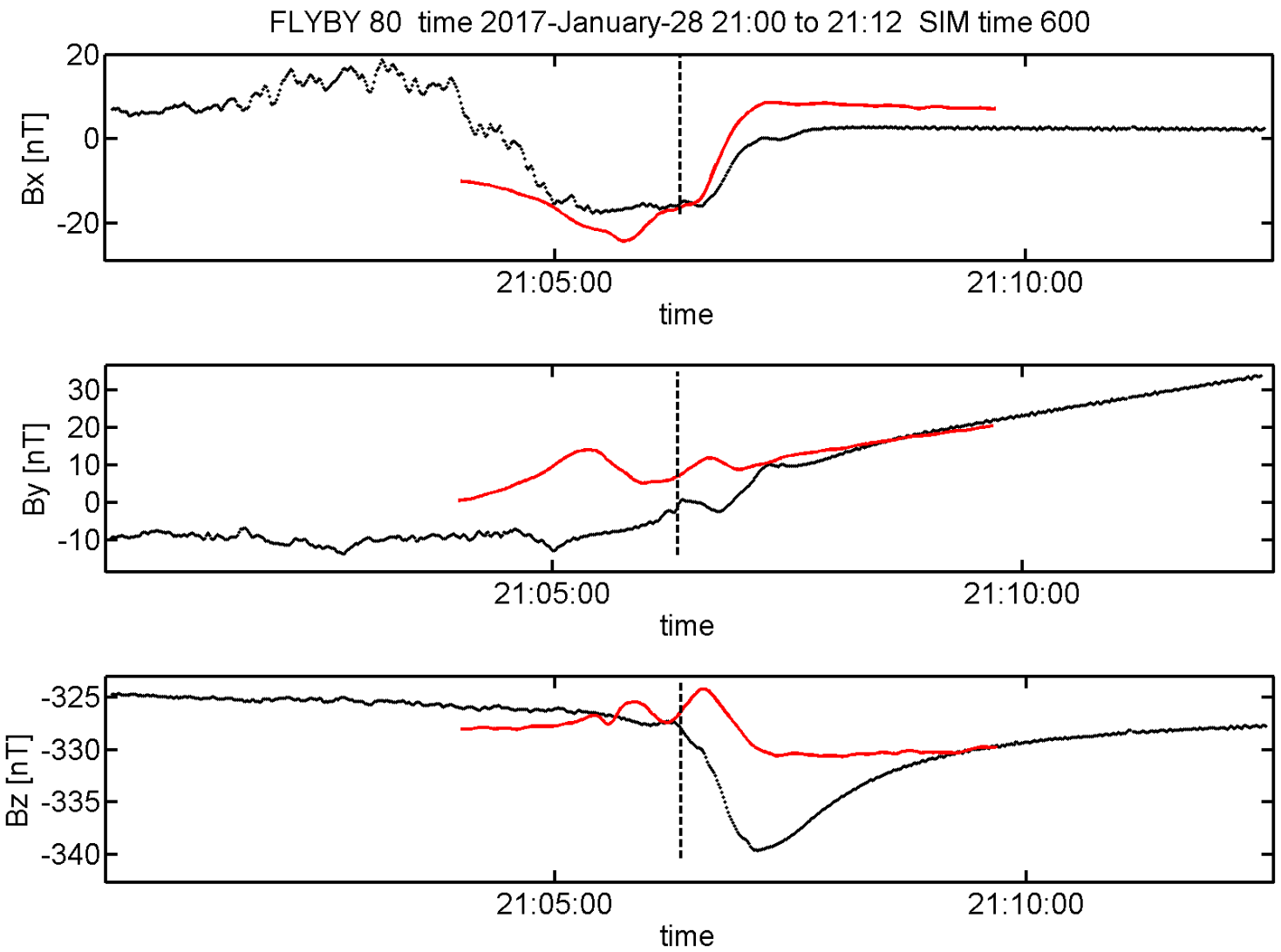

3D Hybrid Simulation - Summary

- model is capable to simulate charge exchange between neutrals and ambient plasma ions
- plasma flow is very slow ($\approx 0.04 v_A$) $\Rightarrow$ large simulation times are needed to reach a steady state
- qualitatively almost similar magnetic signatures for E3, E4 and E11
- poorer agreement for latest flybys E61 and E80 $\Rightarrow$ plume is variable in time?
- ”reversed” signatures for B_y in E11 and E80 - looking for explanations

Global Kinetic Simulations of the Interaction between the Solar Wind and the Moon

Pavel M. Trávníček[1,2], Petr Hellinger[2], David Schriver[1], Stuart D. Bale[3], Petr Šulc[2]

[1]Institute of Geophysics and Planetary Physics, UCLA, Los Angeles, CA, USA
[2]Astronomical Institute and Institute of Atmospheric Physics, ASCR, Prague, Czech
[3]Space Sciences Laboratory, UCB, Berkeley, USA

Fall AGU 2008, San Francisco, USA, December, 2008

Introduction

- When the solar wind interacts with the Moon, plasma is absorbed at the lunar surface leaving a void on the nightside referred to as the wake-tail:
  - No atmosphere and minimal exosphere eliminates the Moon as a source of plasma.
  - The wake-tail is one of the best natural vacuums in the solar system.
- The solar wind IMF passes through the unmagnetized, non-conducting Moon (crustal magnetic fields on the lunar surface may form localized mini-magnetospheres, causing ”limb compressions” in the vicinity of the wake-tail)
- The lunar wake-tail is actively being studied to understand the solar wind refilling processes and its overall three dimensional structure Increasing computer speed and memory can accommodate 2D/3D global hybrid simulations of the solar wind interaction with the Moon.

Observations *in situ*: particles

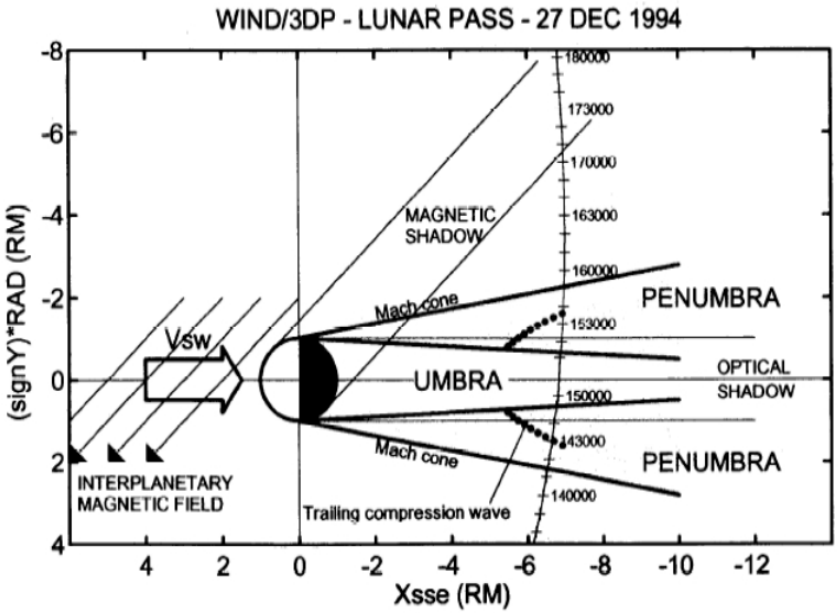

Wind data showed:

density depletion region

e- temperature increase

beams flowing into the depletion region from either side of cavity

enhanced magnetic field in depletion region

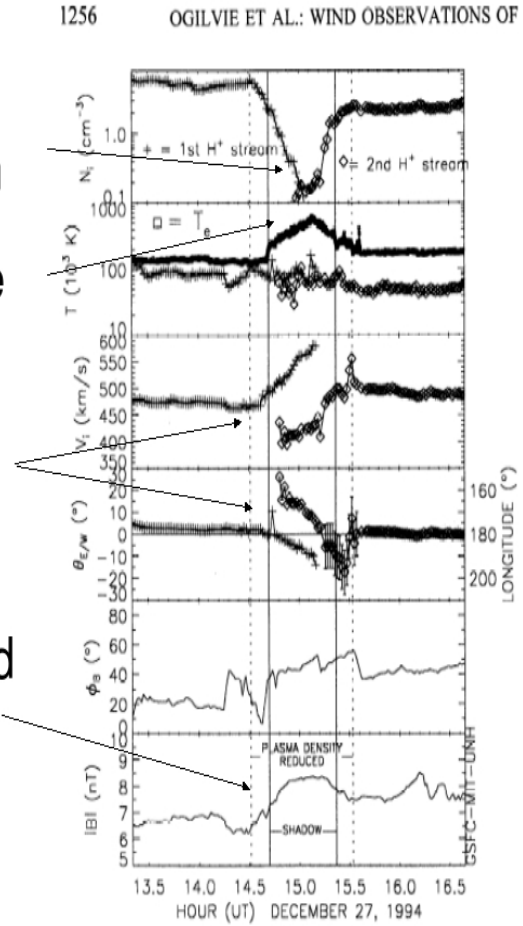

Observations *in situ*: waves

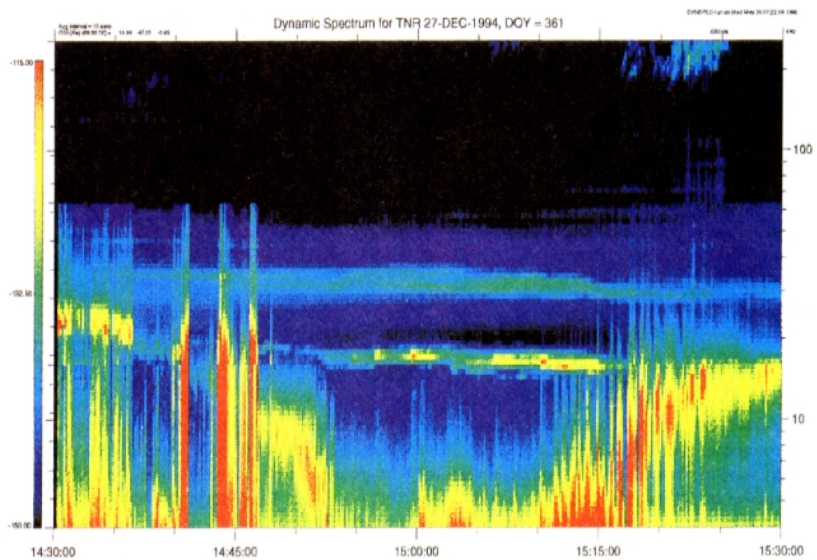

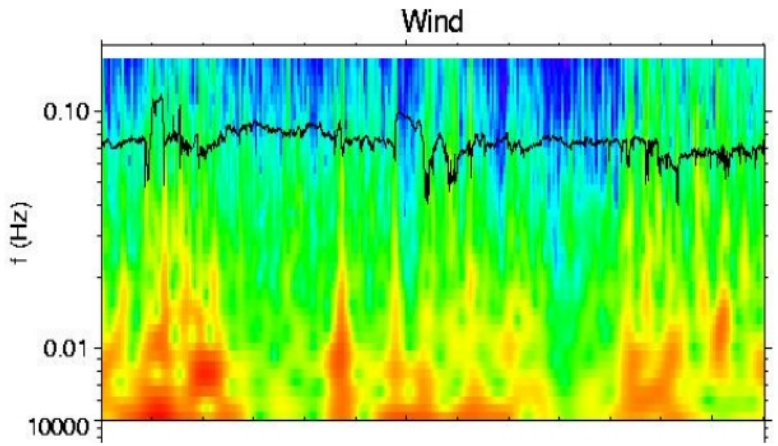

- Plasma waves excited in and arround the density depletion region obseved at ~ 7 R_L by WIND
  [*Farrell et al.*, 1996]
- Ion gyrofrequency waves observed further downstream in the wake-tail ~ 25 R_L by WIND
  [*Travnicek et al.*, 2005]

Observations *in situ*: summary

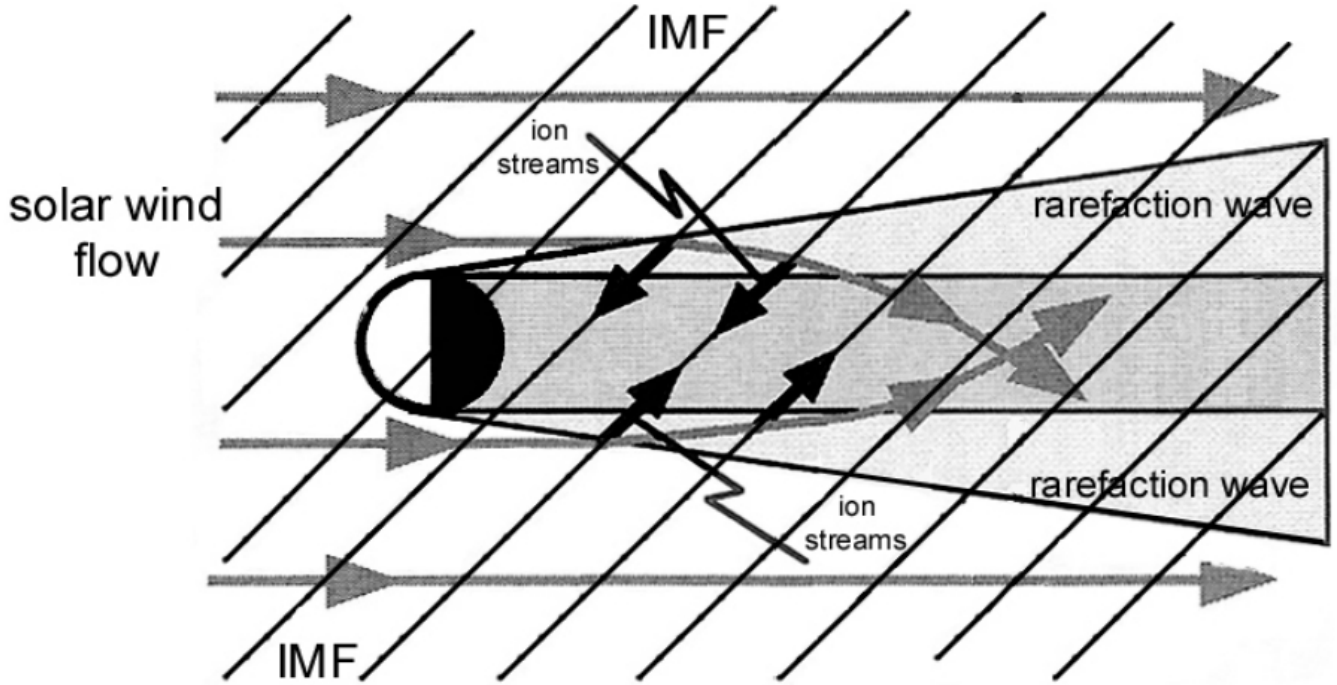

- Observations of streaming and anisotropic plasma distributions, as well as plasma waves of various types indicate that kinetic processes are important in the refilling and formation of the wake-tail.
- We use 2D and 3D global hybrid (kinetic) simulations to model the solar wind interaction with the Moon.

Moon: Simulation results: 2D [Travnicek et al., 2005]

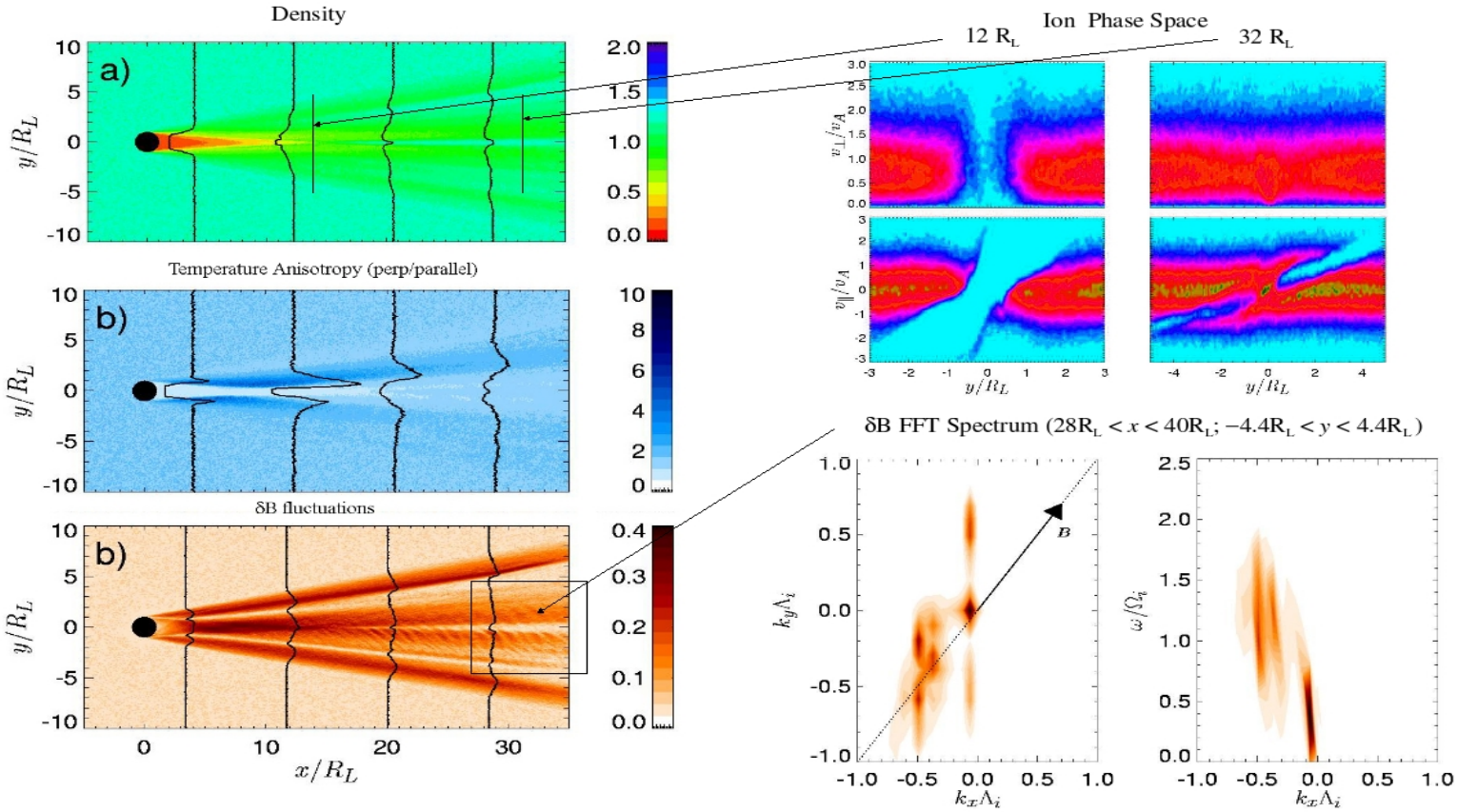

- Cavity in near-moon wake; downstream a density enhacement occurs at center of the depletion region
- Counter-streaming ion distributions in depletion region center; large temperature anisotropies at edges
- Left-hand polarized ion gyrofrequency wave fluctuations in wake-tail

Initialization of the simulation

$n_{\mathrm{sw}} = B_{\mathrm{sw}} = v_{A\mathrm{sw}} = c/\omega_{pp\mathrm{sw}} = \Omega_{p\mathrm{sw}}$	= 1 (a simulation unit)
Spatial resolution $\Delta x = \Delta y = \Delta z$	0.4 $c/\omega_{pp\mathrm{sw}}$
Temporal resolution (time step) Δt	0.02 $\Omega_{p\mathrm{sw}}^{-1}$
Spatial size of the system $L_x/L_y = L_z$	80 / 200 $c/\omega_{pp\mathrm{sw}}$
Total simulation time	80.0 $\Omega_{p\mathrm{sw}}^{-1}$
$\beta_{p\mathrm{sw}}$ / $\beta_{e\mathrm{sw}}$	1.0 / 1.0
Number of macro-particles per cell	40
Total number of macro-particles	$\sim 0.8\times10^9$
Solar wind velocity v_{sw}	5.0 $v_{A,\mathrm{sw}}$
Orientation of IMF in (X, Y) plane	- 45°
Radius of the Moon R_L	12 $c/\omega_{pp\mathrm{sw}}$

Results: Plasma density n_p/n_{psw}

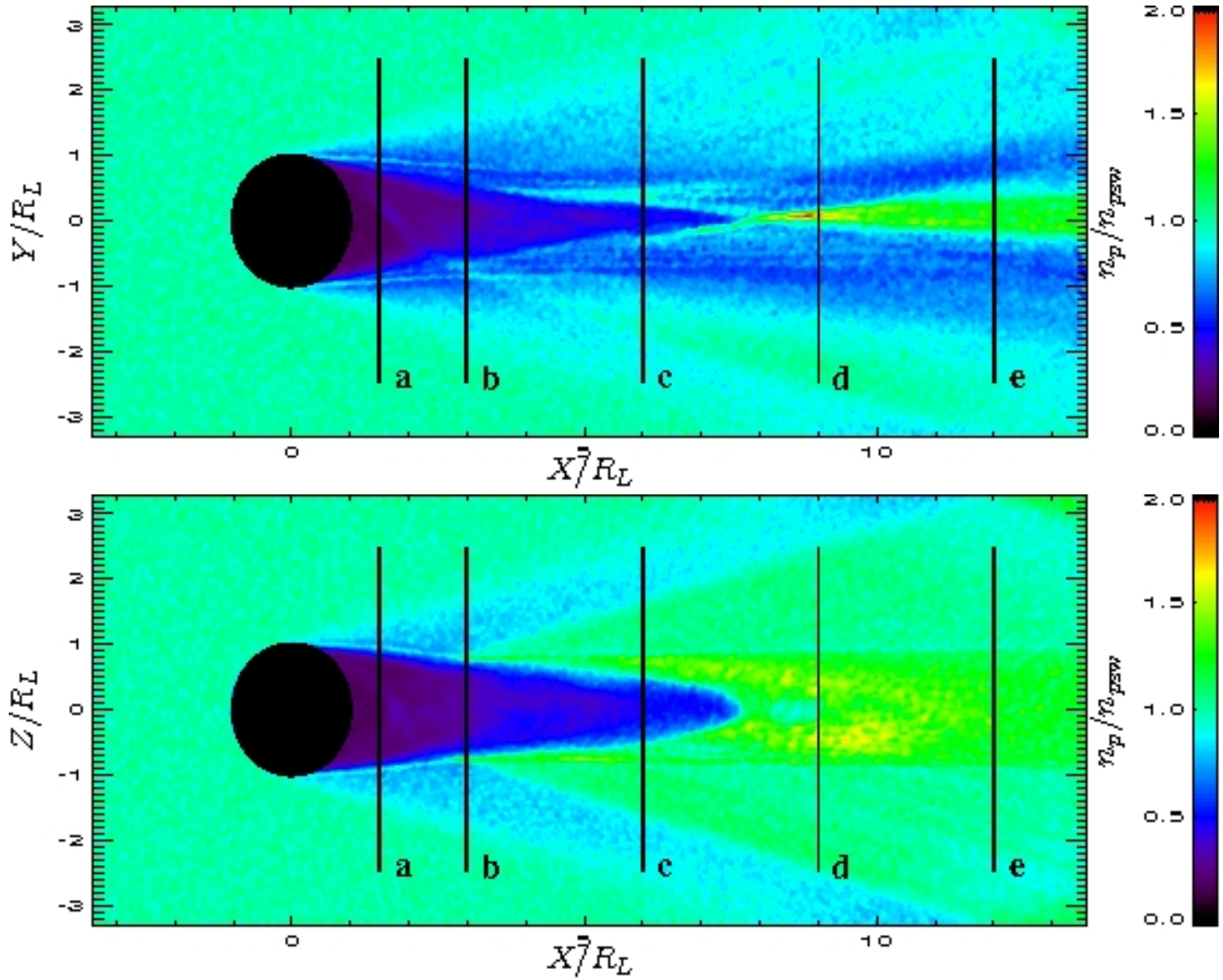

Results: Plasma density n_p/n_{psw}

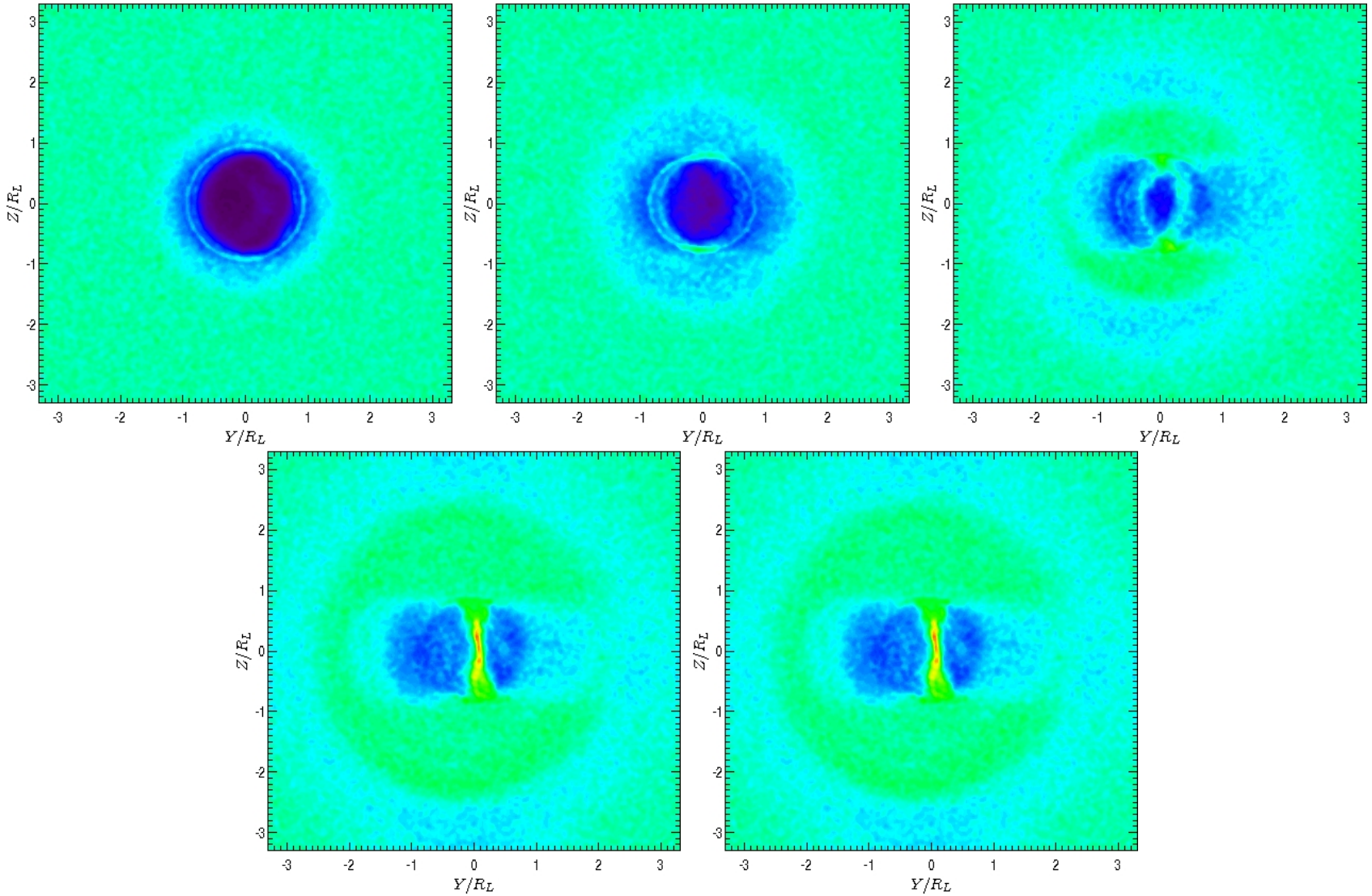

Density contours in a set of $(X = X_0, Y, Z)$ planes for $X_0 = 1.5\ R_L$, $3\ R_L$, $6\ R_L$, $9\ R_L$, and $12\ R_L$.

Results: Magnetic field $\boldsymbol{B}/B_{\mathrm{sw}}$

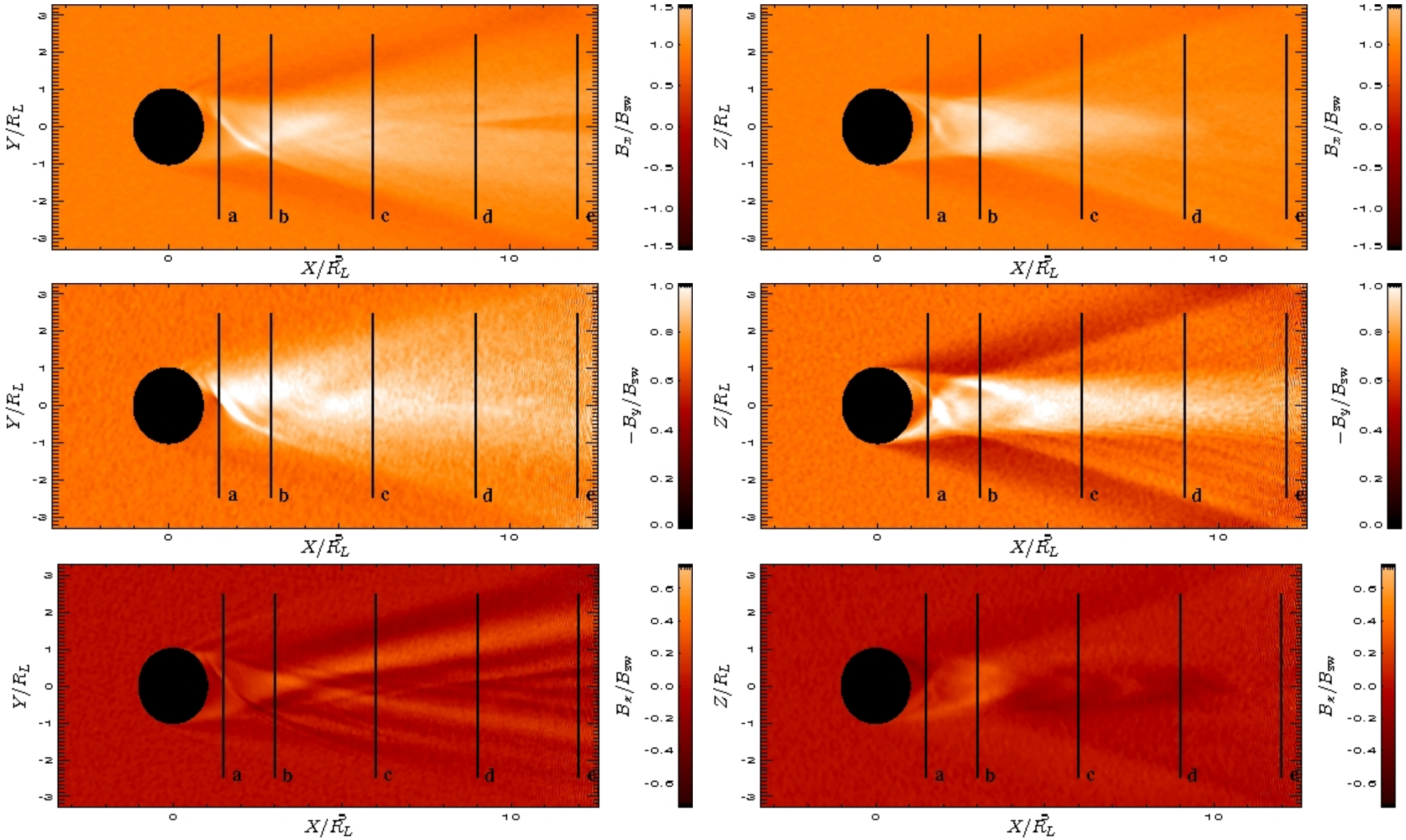

Results: Plasma bulk speed v/v_{Asw}

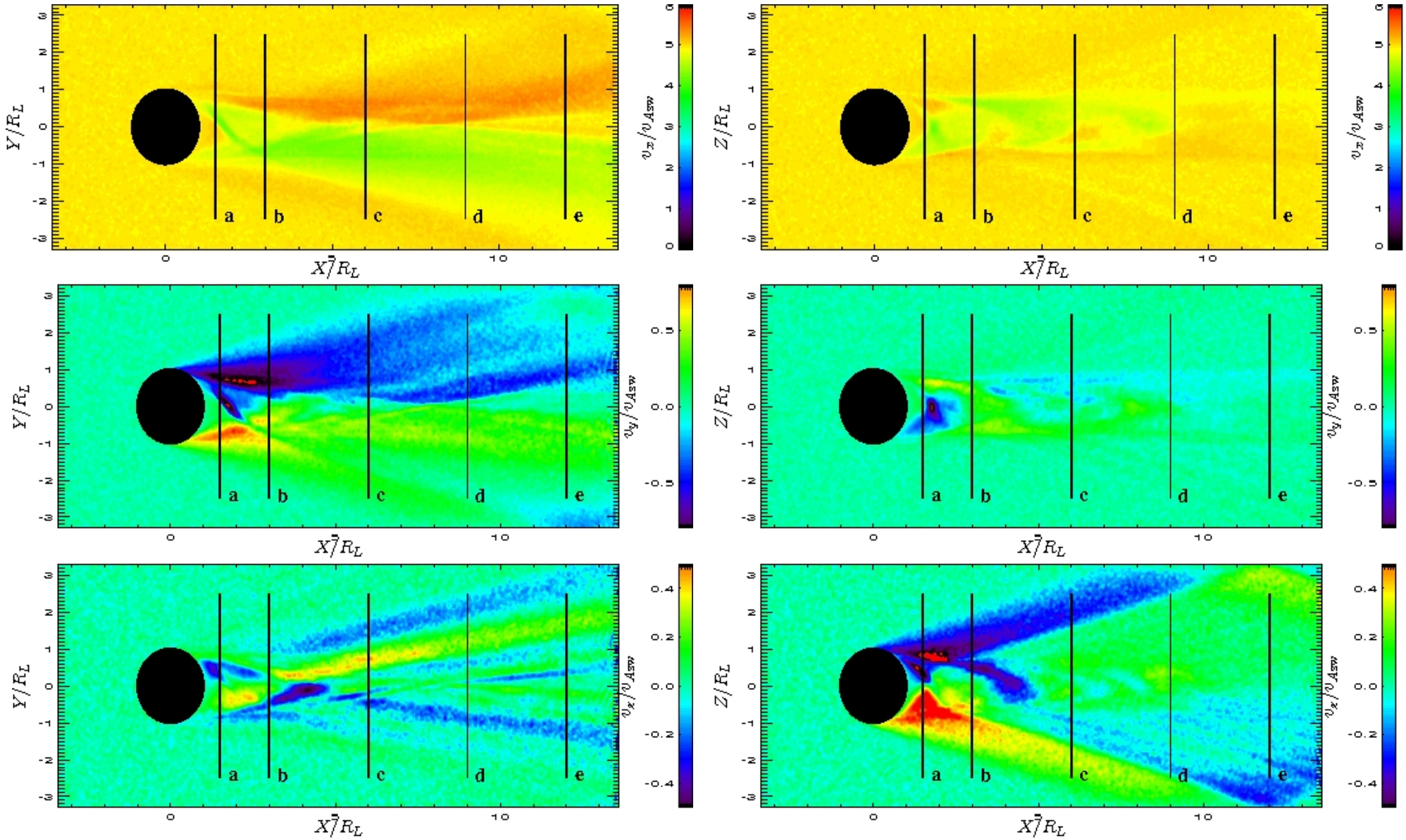

Results: Temperature anisotropy $T_\perp/T_{||}$

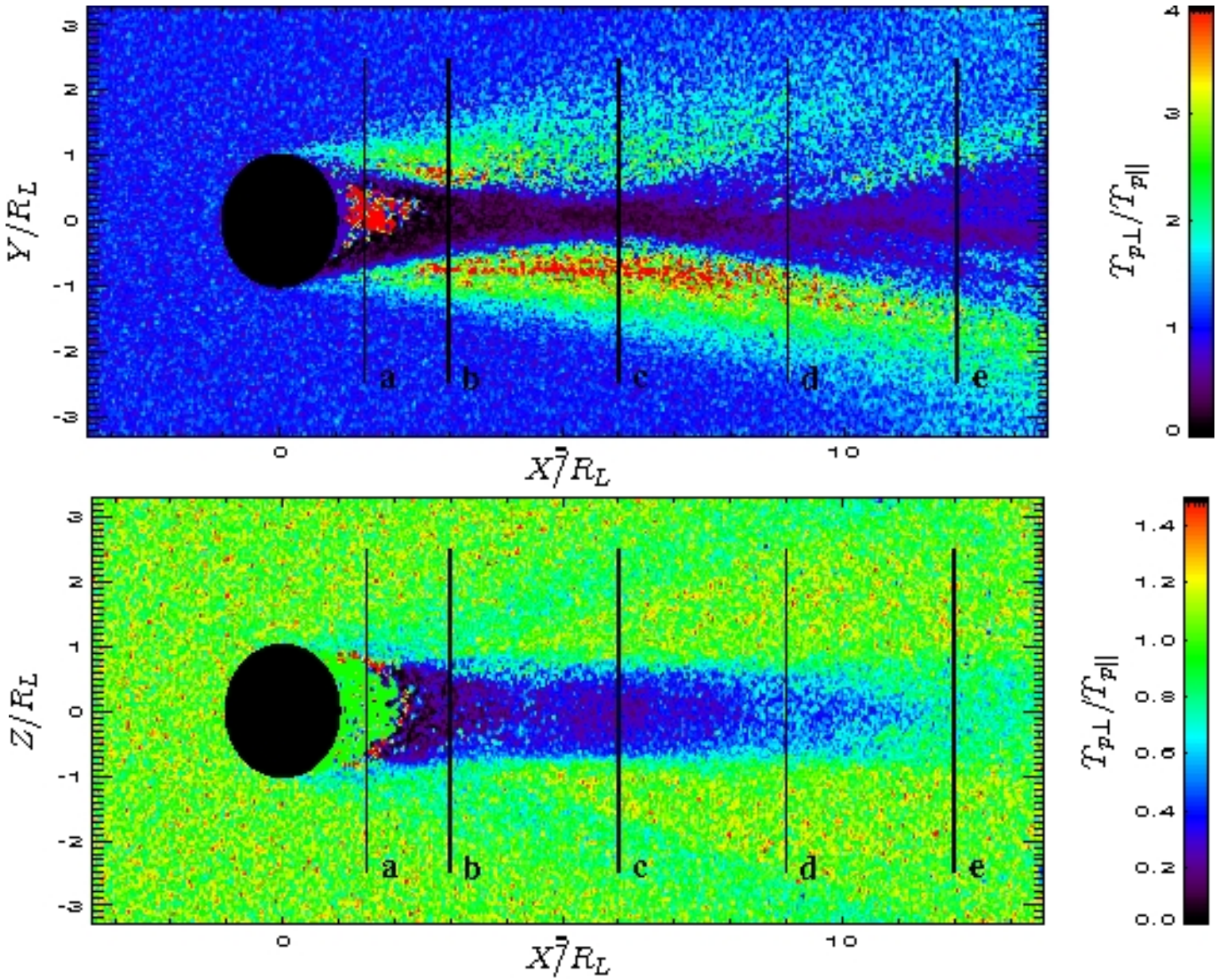

Results: Temperature Anisotropy $T_\perp/T_\parallel$

Contours of the temperature anisotropy $T_\perp/T_\parallel$ in a set of $(X = X_0, Y, Z)$ planes for $X_0 = 1.5\ R_L$, $3\ R_L$, $6\ R_L$, $9\ R_L$, and $12\ R_L$:

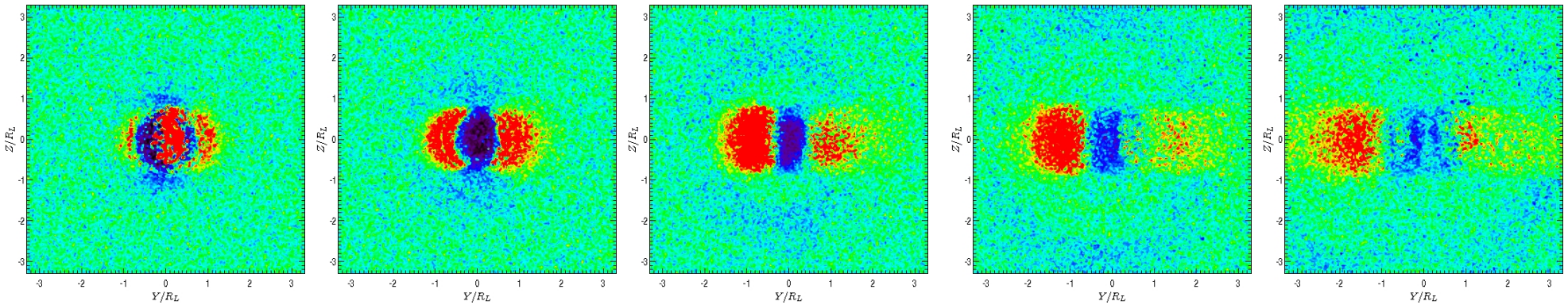

Plasma state shown in the form of a set of histograms in $(\beta_{p\parallel}, T_\perp/T_\parallel)$ space for $X_0 = 1.5\ R_L$, $3\ R_L$, $6\ R_L$, $9\ R_L$, and $12\ R_L$:

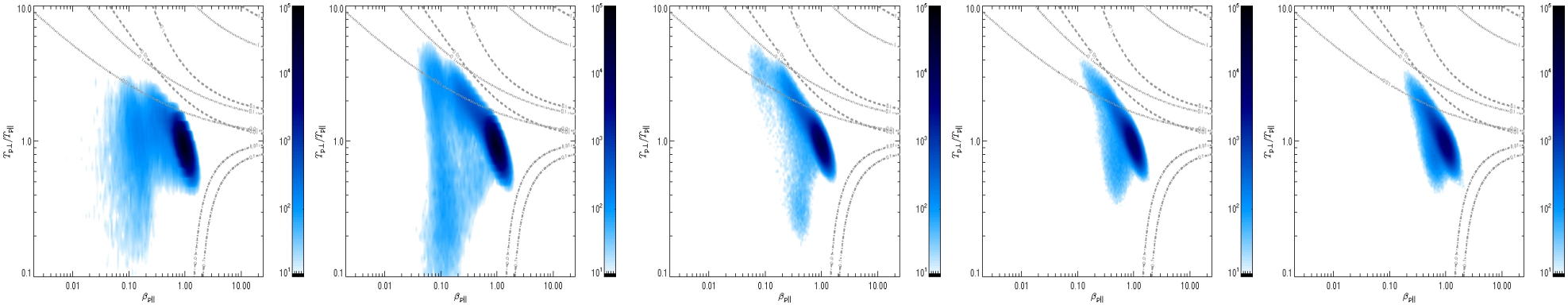

Conclusions

- Wake refilling is described by a magnetized plasma to vacuum expansion with plasma flow primarily in the magnetic field aligned direction.
- Faster electrons move ahead of protons towards cavity center. The charge separation causes electric field that accelerates protons.
- The current associated with the plasma to vacuum expansion leads to an enhancement of the magnetic field inside the plasma depletion region.
- The rate of the plasma refilling process depends on the solar wind speed, plasma temperature and IMF orientation.
- The refilling process is ongoing in the plane defined by the flow direction and IMF. The IMF lines provide the collisionless plasma access to the wake center.
- The density cavity is filled with ion beams counterstreaming along magnetic field lines; at the cavity's edge the plasma is anisotropic in temperature ($T_{p\parallel} \neq T_{p\perp}$)

Conclusions

- Density enhancement bump forms in center of far downstream wake due to counterstreaming beams.
- Asymmetries form in the density depletion region because of the skewed IMF orientation with respect to solar wind flow direction. These asymmetries form in the distribution of the plasma (density) and also in the distribution of the temperature anisotropy across the lunar wake.
- Sections of the lunar wake at lower down-tail distances ($X < 6\ R_L$ in our case) contain plasma with wider spread of the effective temperature anisotropy $T_{\mathrm{p}\perp}/T_{\mathrm{p}\parallel}$. The center of the wake contains beaming plasma ($T_{\mathrm{p}\perp} < T_{\mathrm{p}\parallel}$) while edges of the wake along Y-direction contain plasma with $T_{\mathrm{p}\perp} > T_{\mathrm{p}\parallel}$. Further down-tail the plasma gets more mixed and is more isotropic.

Kinetic Simulation of Mercury's Magnetosphere Compared with Observations During MESSENGER's First Mercury Flybys on 14 January 2008 and 6 October 2008

P. M. Trávníček[1,2], P. Hellinger[2], D. Schriver[1], D. Herčík[2], J. Páral[2,3], B. J. Anderson[4], S. M. Krimigis[4], R.L. McNutt Jr.[4], M. Sarantos[5], J. A. Slavin[5], S. C. Solomon[6] T. H. Zurbuchen[7]

[1]Institute of Geophysics and Planetary Physics, UCLA, Los Angeles, CA, USA; [2]Astronomical Institute and Institute of Atmospheric Physics, ASCR, Prague, Czech Republic; [3]Department of Physics, UoA, Edmonton, Canada; [4]Heliophysics Science Division, NASA GSFC, Greenbelt, MD, USA; [5]The Johns Hopkins University Applied Physics Laboratory, Laurel, MD, USA; [6]Department of Terrestrial Magnetism, Carnegie Institution of Washington, D.C; [7]Department of Atmospheric, Oceanic, and space Sciences, University of Michigan, Ann Arbor, MI, USA.

Fall AGU 2008, San Francisco, USA, December, 2008

Mercury observations *in situ*

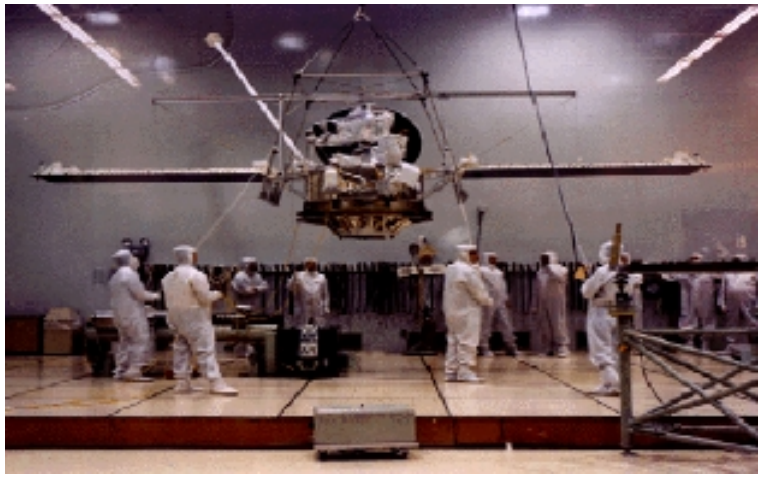

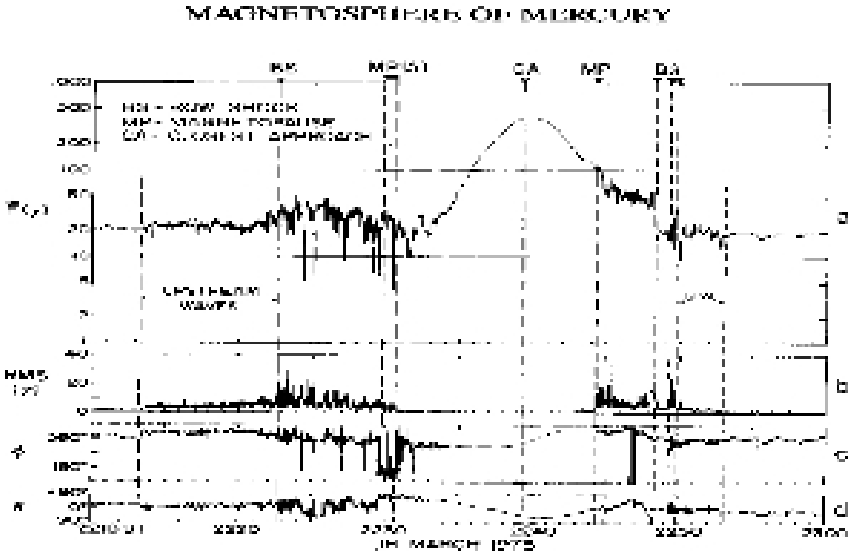

- Mercury is smaller than Earth and is typically embedded in a denser solar wind plasma
- Untill January 14 2008, Mercury has been observed by single spacecraft (Mariner 10) in the 1970's (two encounters)
- Both encounters have shown, that Mercury has a weak intrinsic magnetic field and magnetosphere
- Mercury orbits Sun on an excentric orbit causing significant changes in its magnetosphere
- New probes: MESSENGER (NASA), BepiColombo (ESA)

Mercury observations *in situ*

- Magnetic dipole moment from Mariner 10 has been estimated to be between 170 nT R_M^3 ($\approx 2.5 \cdot 10^{19}$ Am^2) [*Jackson and Beard*, 1977] and 349 nT R_M^3 ($\approx 5. \cdot 10^{19}$ Am^2) [*Ness et al.*, 1975]. MESSENGER 1st and 2nd flybys: 250 nT R_M^3.
- The magnetopause nose standoff distance has been estimated to be between 1.3 and 2.1 R_M for Mariner and MESSENGER flybys.
- Mariner 10 electron data indicated that a substorm-like event may have occurred, suggesting magnetic reconnection in magnetotail [*Siscoe et al.*, 1975; *Eraker and Simpson*, 1986]. MESSENGER 2nd flyby shows evidence of strong magnetic reconnection.
- Small Mercury's magnetosphere can be exposed to solar wind with speeds ranging from 200 km/s up to 600 km/s [*Russell et al.*, 1988]. MESSENGER 1st and 2nd flyby: $v_{\mathrm{sw}} \approx 400$ km/s.

Schematic of Mercury's magnetosphere

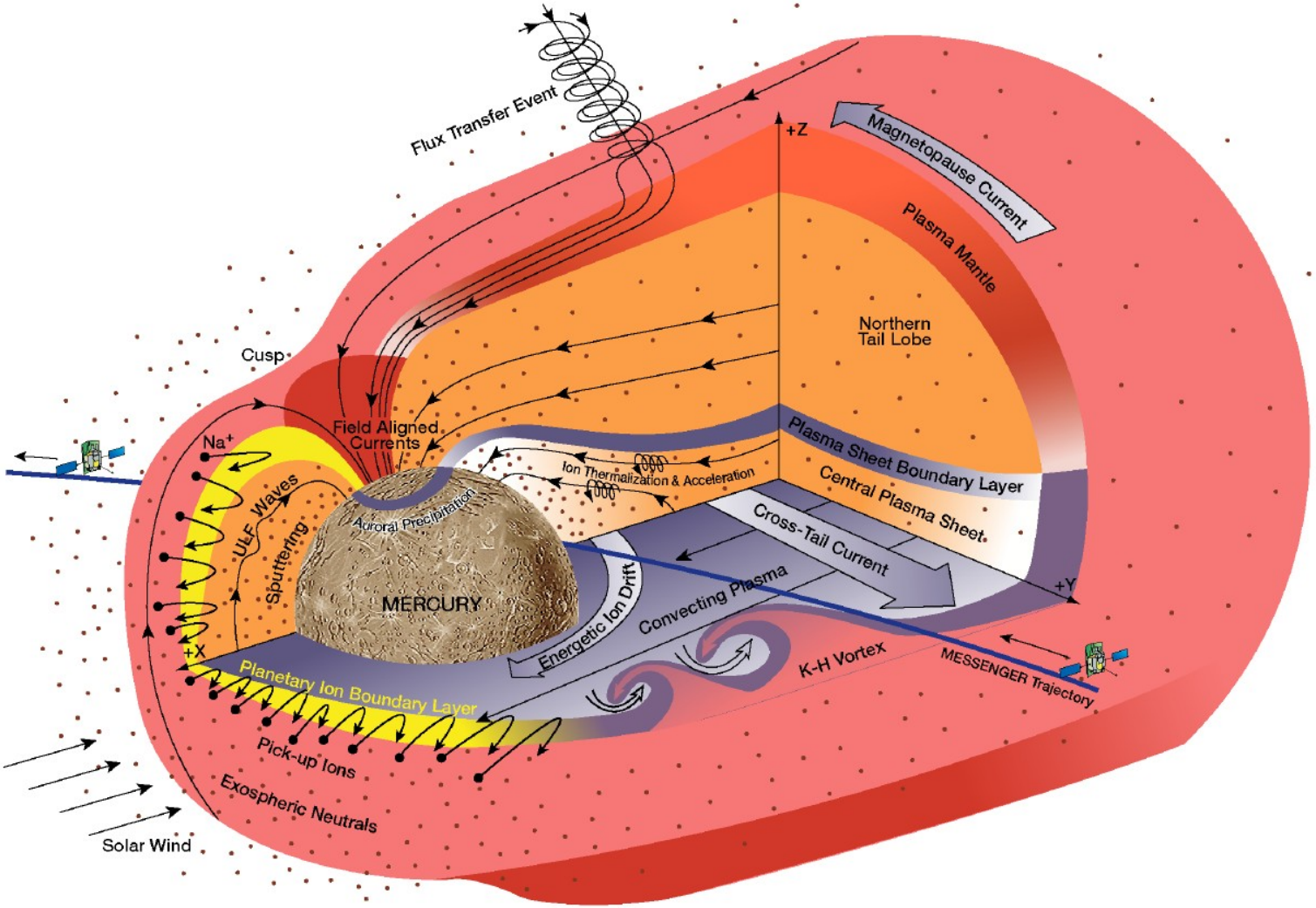

[*Slavin et al.*, 2008]

Global simulations to date

All (global) numerical models / techniques employ some compromises:

- MHD 3D simulations [*Kabin et al.*, 2001].
- Hybrid models with spatial resolution of several c/ω_{pi} [*Kalio and Janhunen*, 2003] (typical Larmor radius at Mercury is 2-3 c/ω_{pi}).
- Global 2D hybrid models of solar wind interacting with magnetized obstacles have been also considered [*Omidi et al.*, 2002].
- **Scaled down model with spatial resolution of the order c/ω_{pi} and reasonable ratio between Larmor radius and the scaled down size of the planet** [*Travnicek et al.*, 2007].

Scaling down the model

- We use a scaled down model of Mercury with a magnetic moment $M = 50,000 B_{\mathrm{sw}} (c/\omega_{pp\mathrm{sw}})^3 4\pi/\mu_0 = 3.76 \cdot 10^{19}/\varepsilon$ Am^2 for both studies.
- The downscaling preserves the stand-off distance of the magnetopause predicted by $R_{\mathrm{mp}} = (2B_{\mathrm{eq}}^2/(\mu_0 P_{\mathrm{ram,sw}}))^{1/6} R_M$, where B_{eq} is the magnetic field at the equator of the planet with radius R_M and $P_{\mathrm{ram,sw}}$ is solar wind ram pressure $n_{\mathrm{sw}} m_p v_{\mathrm{sw}}^2$, where m_p is the proton mass ($m_p = 1$ in simulation units).
- Although scaled down, the radius R_M is always sufficiently larger than the local Larmor radius r_L. The scaling factor of the physical space equals to 3-4.

Wave-particle interaction

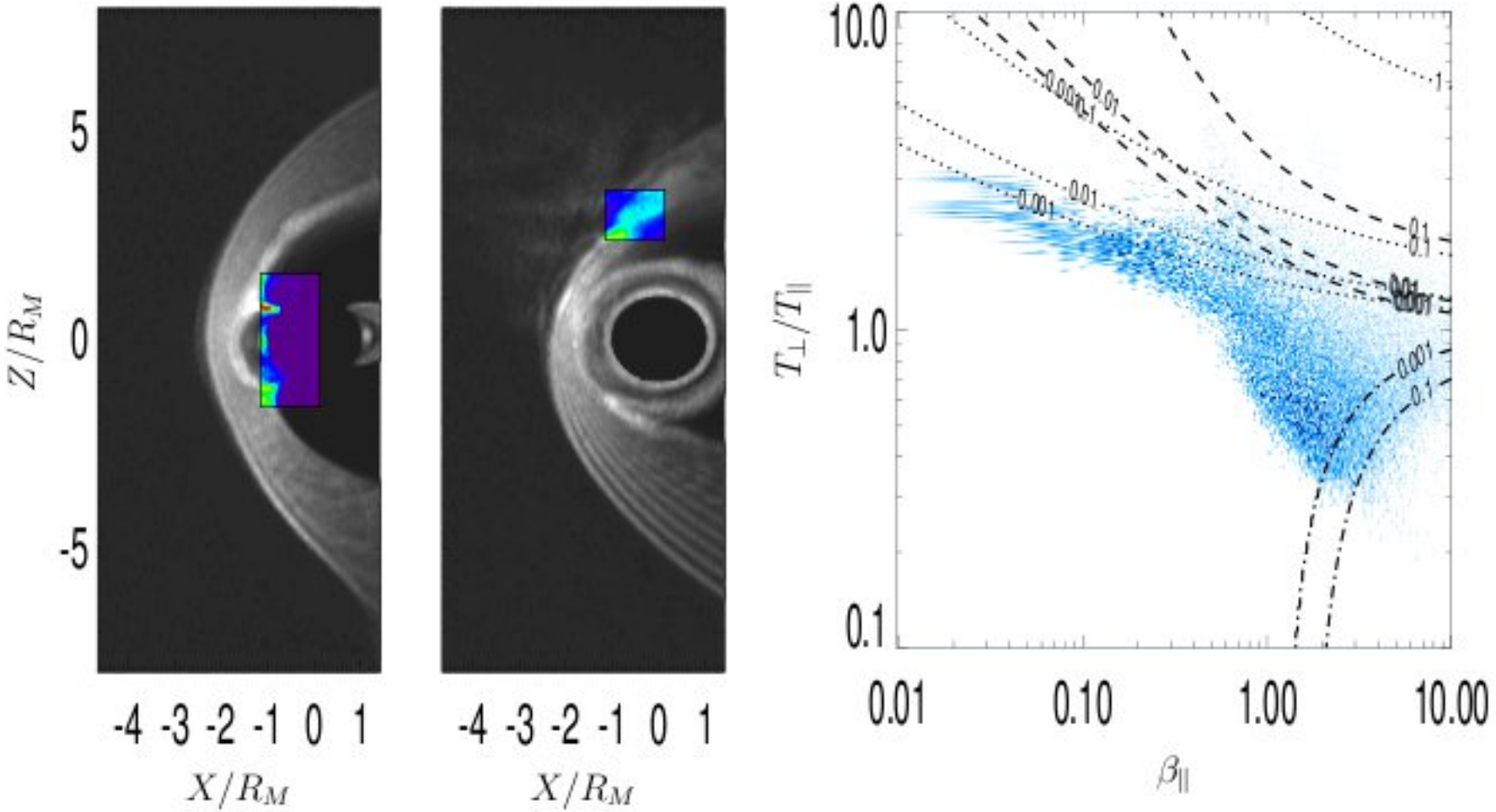

Our model self-consistently resolves exchange of energy between particles and waves.

Protons ejected from Hermean surface

We injected H^+ ions into the system from the planetary surface to include a zero-order model of ions sputtered of the surface. These ions were injected with density of the order $n_p \sim 10^{-4}\, n_{\mathrm{sw}}$ isotropically from Mercury's surface in both cases with velocity $v_p \sim 0.05\, v_A$ perpendicular to the surface.

Protons ejected from Hermean surface:
$v_{psw} = 5v_{Asw}$ vs. $v_{psw} = 3v_{Asw}$

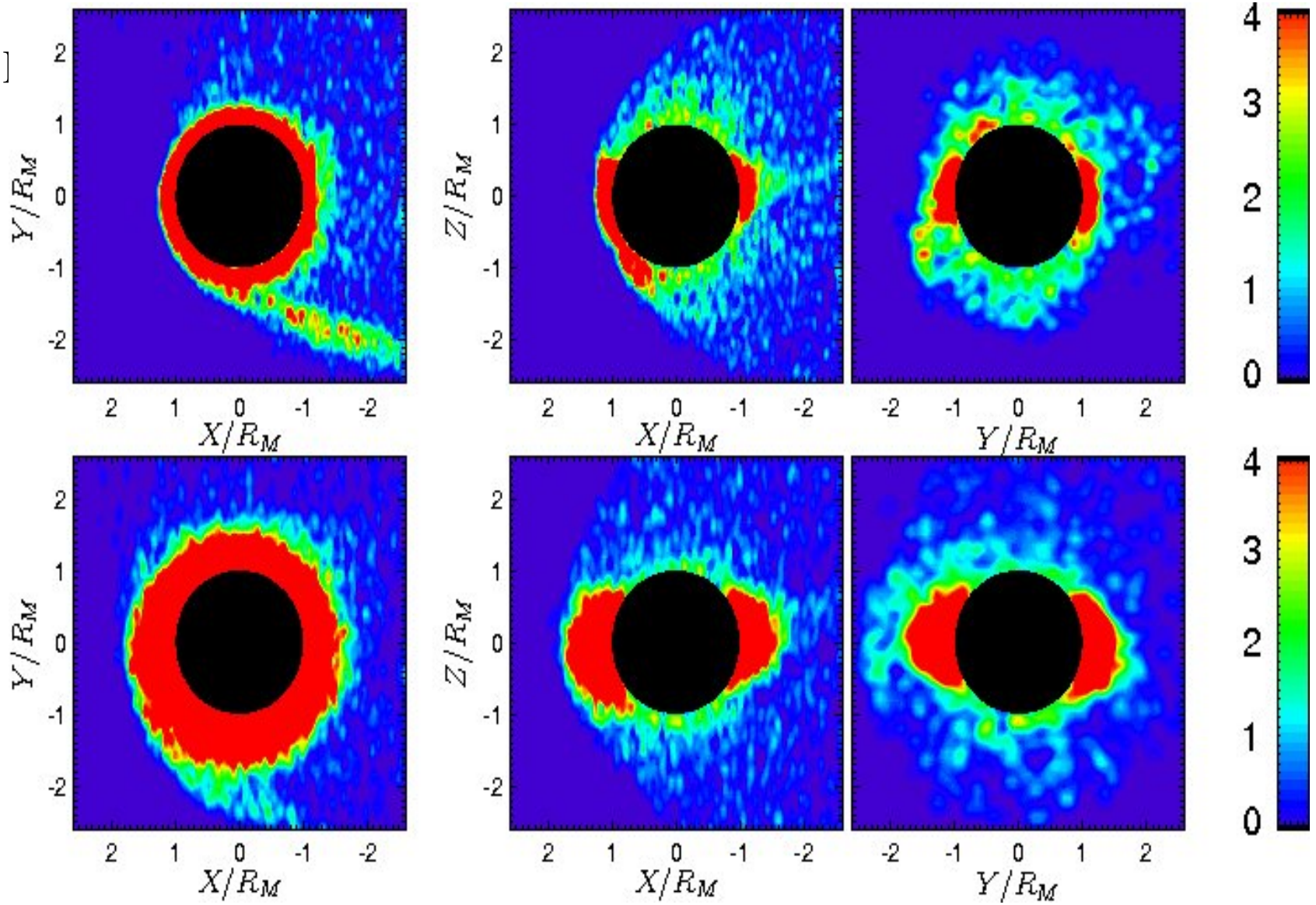

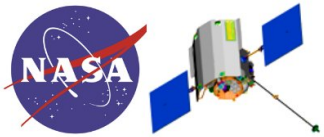

Flyby 1 (north-ward IMF): Model initialization

$n_{\rm sw} = B_{\rm sw} = v_{A\rm sw} = c/\omega_{p\rm sw} = \Omega_{p\rm sw}$	= 1 (a simulation unit)
Spatial resolution $\Delta x/\Delta y = \Delta z$	0.4/1.0 $c/\omega_{pp\rm sw}$
Temporal resolution (time step) Δt	0.02 $\Omega_{p\rm sw}^{-1}$
Spatial size of the system $L_x/L_y = L_z$	260 / 288 $c/\omega_{p\rm sw}$
Total simulation time	100.0 $\Omega_{p\rm sw}^{-1}$
$\beta_{p\rm sw}$ / $\beta_{e\rm sw}$	1.0 / 1.0
Number of macro-particles per cell	70
Total number of macro-particles	$\sim 3.2\times10^9$
Solar wind velocity $v_{\rm sw}$	4.0 $v_{A,\rm sw}$
Orientation of IMF in (X,Z) plane	+ 20° (north-ward IMF)
Mercury's magnetic moment M_M	250 nT R_M^3 (no tilt)

Flyby 1 (north-ward IMF): Simulated density n_p/n_{psw}

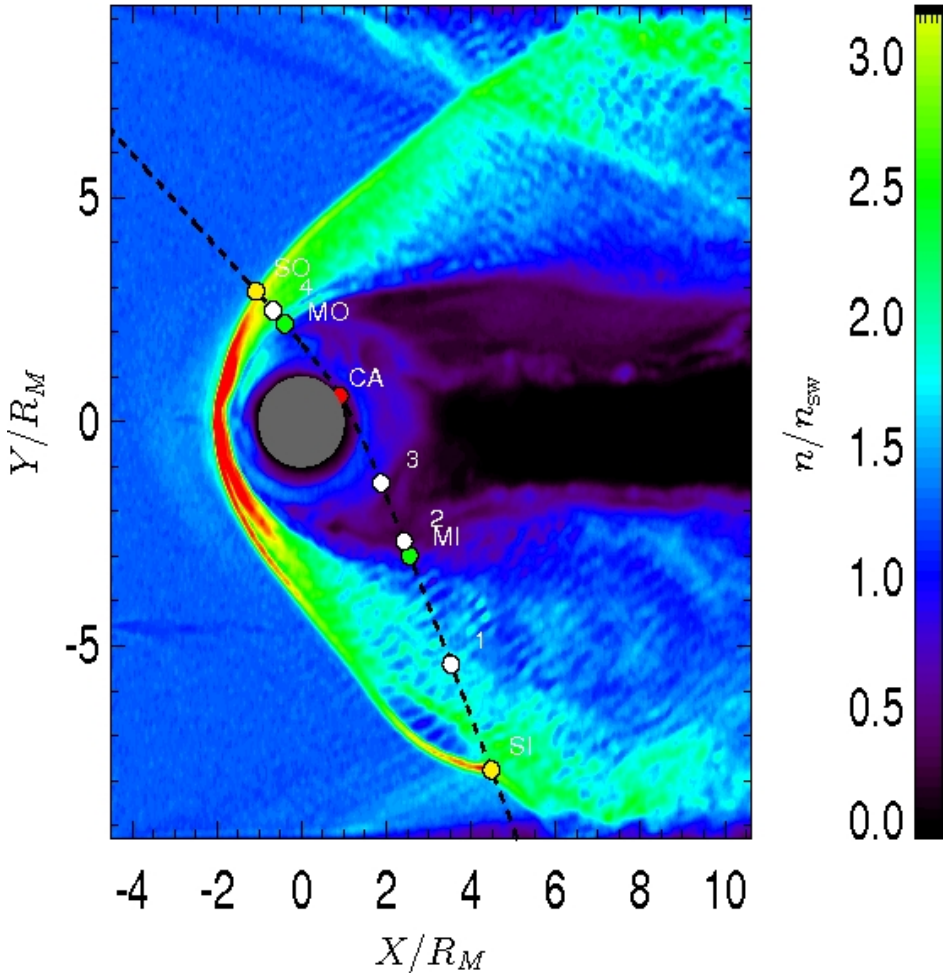

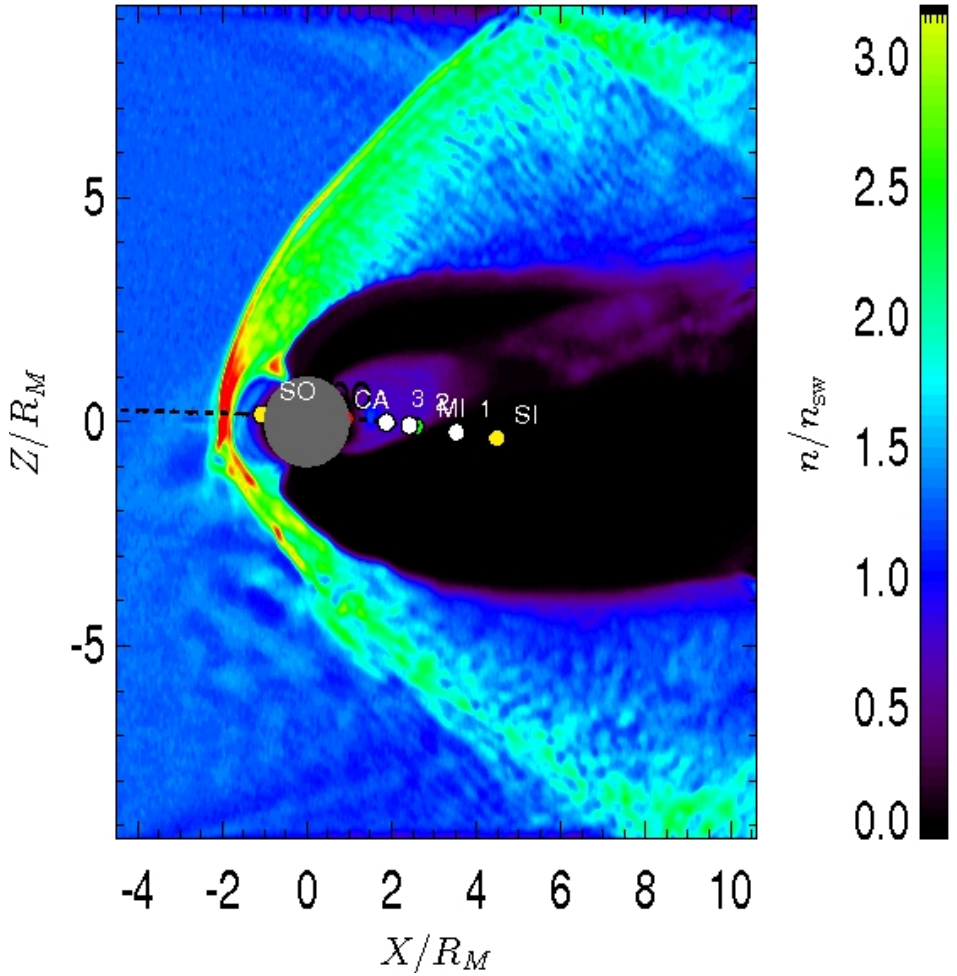

Flyby 1 (north-ward IMF): Simulated n_p/n_{psw}

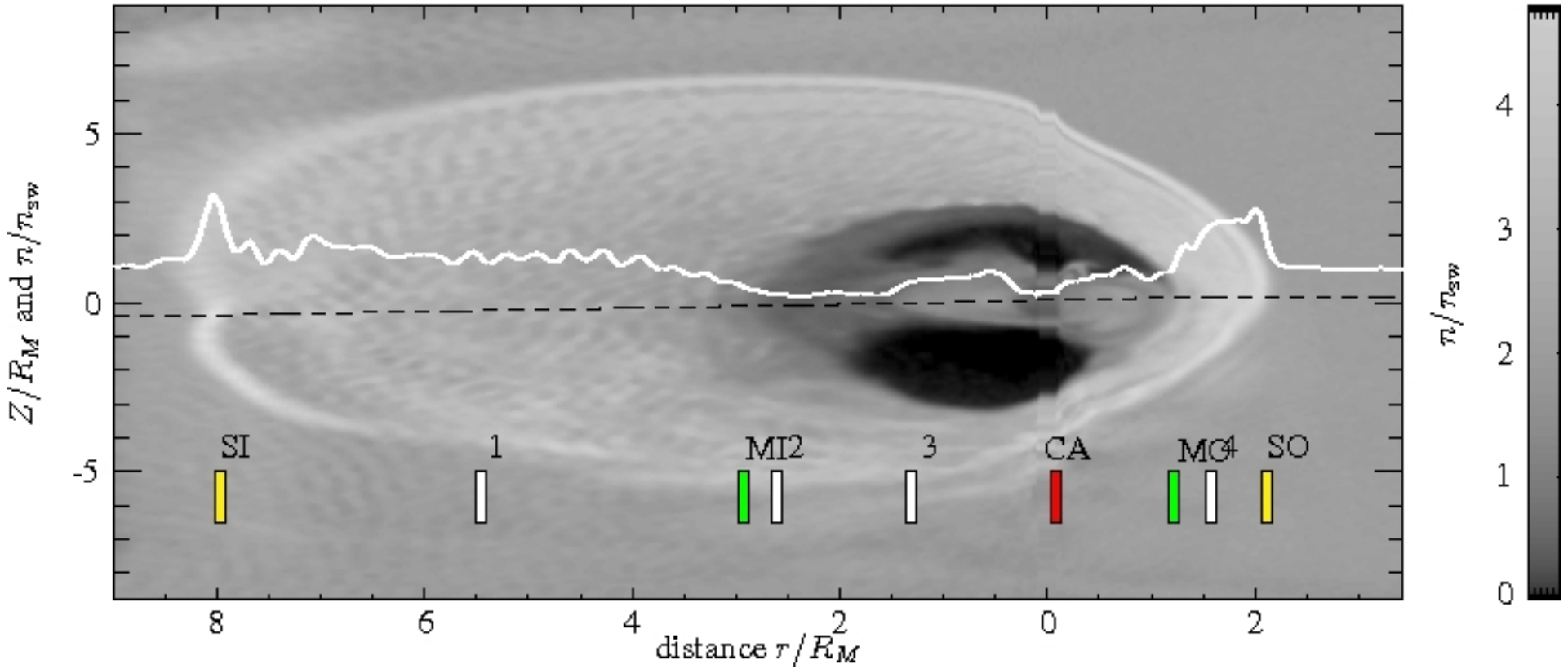

Flyby 1 (north-ward IMF): Simulated B/B_{sw}

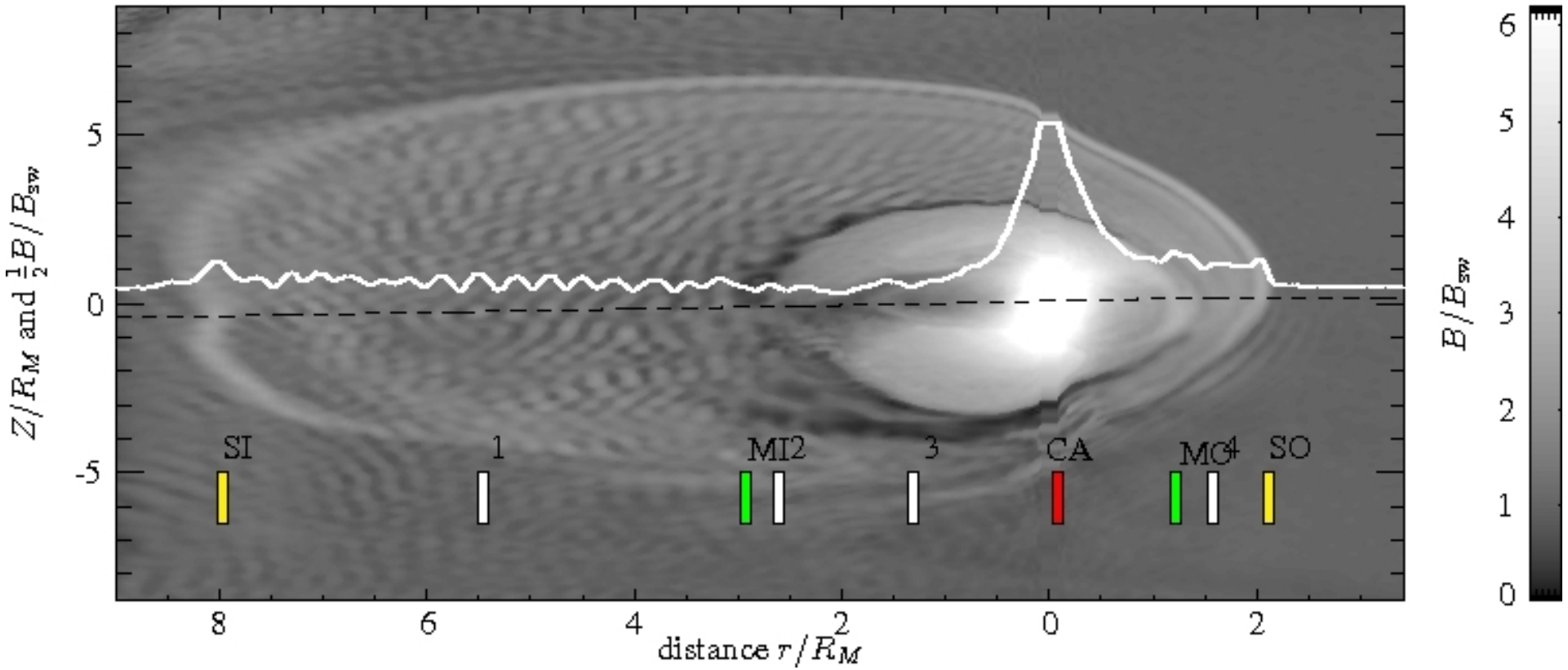

Flyby 1 (north-ward IMF): virtual and *in situ* measurements

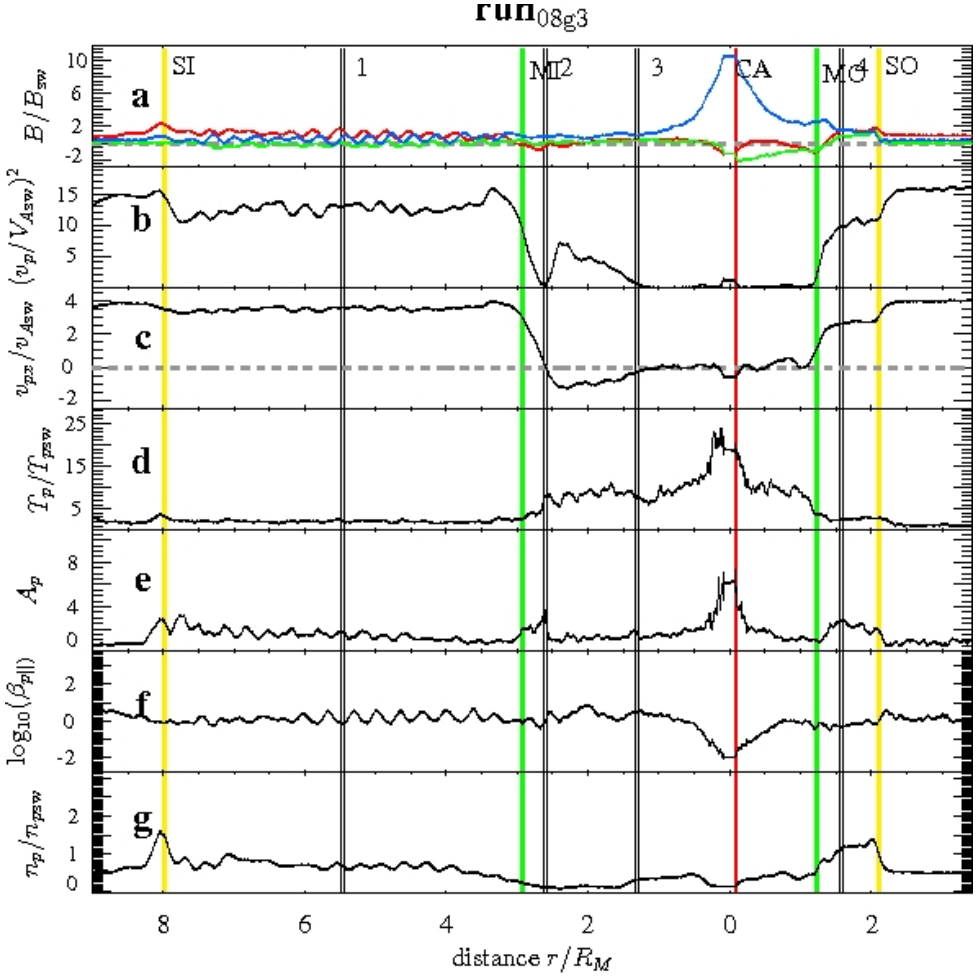

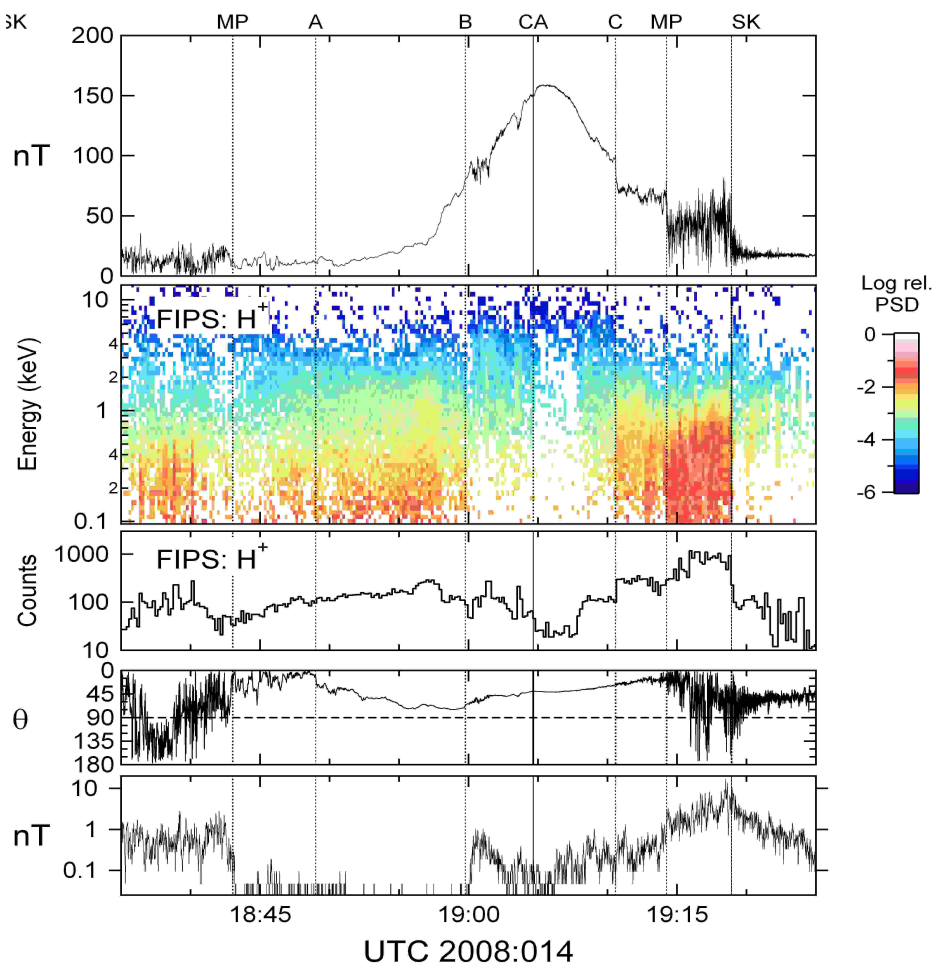

LEFT: virtual observations

RIGHT: MAG and FIPS *in situ* observations

Flyby 1 (north-ward IMF): S/C trajectory in $(\beta_{p||}, T_{p\perp}/T_{p||})$ space

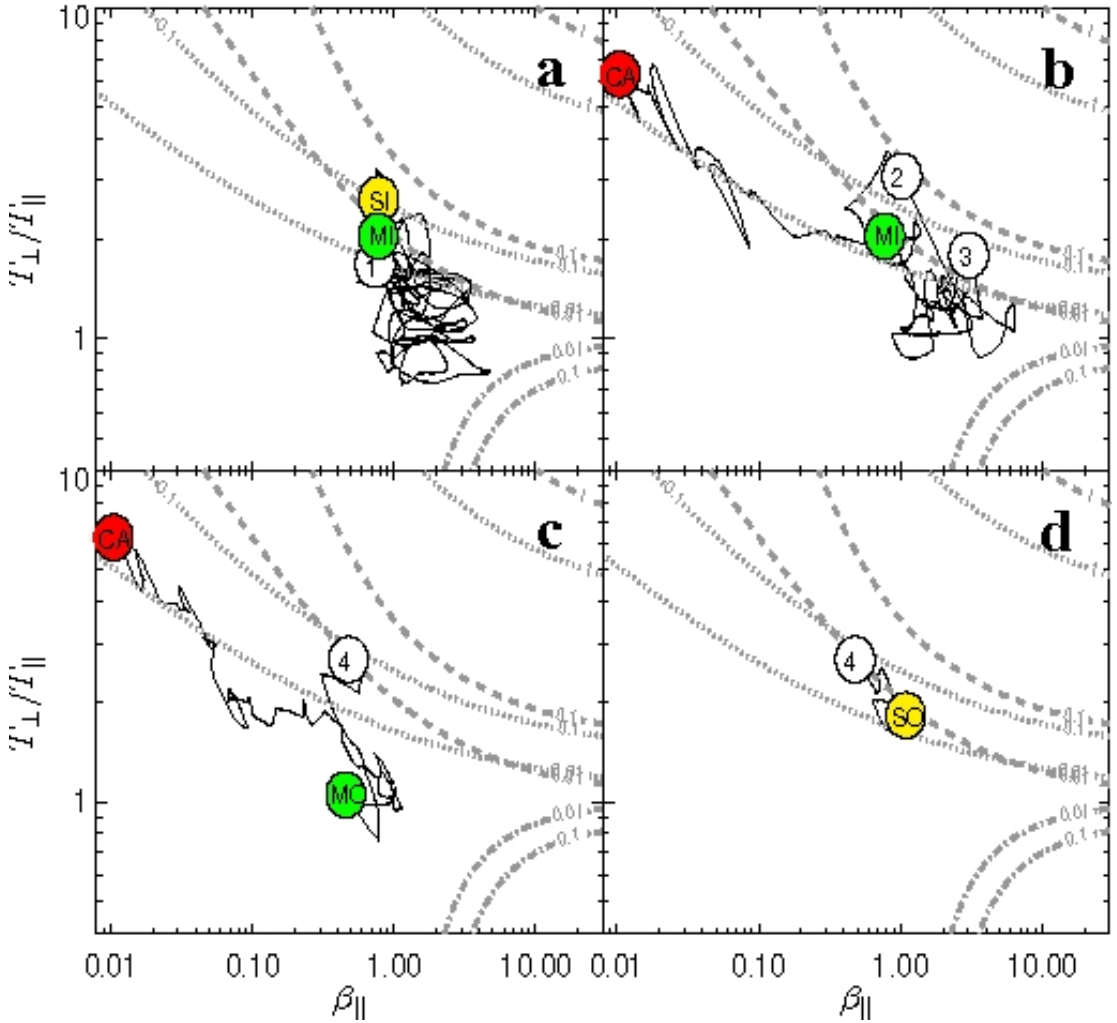

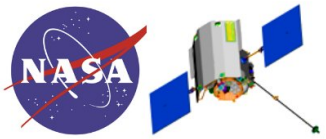

Flyby 2 (south-ward IMF): Model initialization

$n_{\rm sw} = B_{\rm sw} = v_{A\rm sw} = c/\omega_{p\rm sw} = \Omega_{p\rm sw}$	= 1 (a simulation unit)
Spatial resolution $\Delta x/\Delta y = \Delta z$	0.4/1.0 $c/\omega_{pp\rm sw}$
Temporal resolution (time step) Δt	0.02 $\Omega_{p\rm sw}^{-1}$
Spatial size of the system $L_x/L_y = L_z$	260 / 288 $c/\omega_{p\rm sw}$
Total simulation time	100.0 $\Omega_{p\rm sw}^{-1}$
$\beta_{p\rm sw}$ / $\beta_{e\rm sw}$	1.0 / 1.0
Number of macro-particles per cell	70
Total number of macro-particles	$\sim 3.2\times10^9$
Solar wind velocity $v_{\rm sw}$	4.0 $v_{A,\rm sw}$
Orientation of IMF in (X,Z) plane	- 20° (south-ward IMF)
Mercury's magnetic moment M_M	250 nT R_M^3 (no tilt)

Flyby 2 (south-ward IMF): Simulated density n_p/n_{psw}

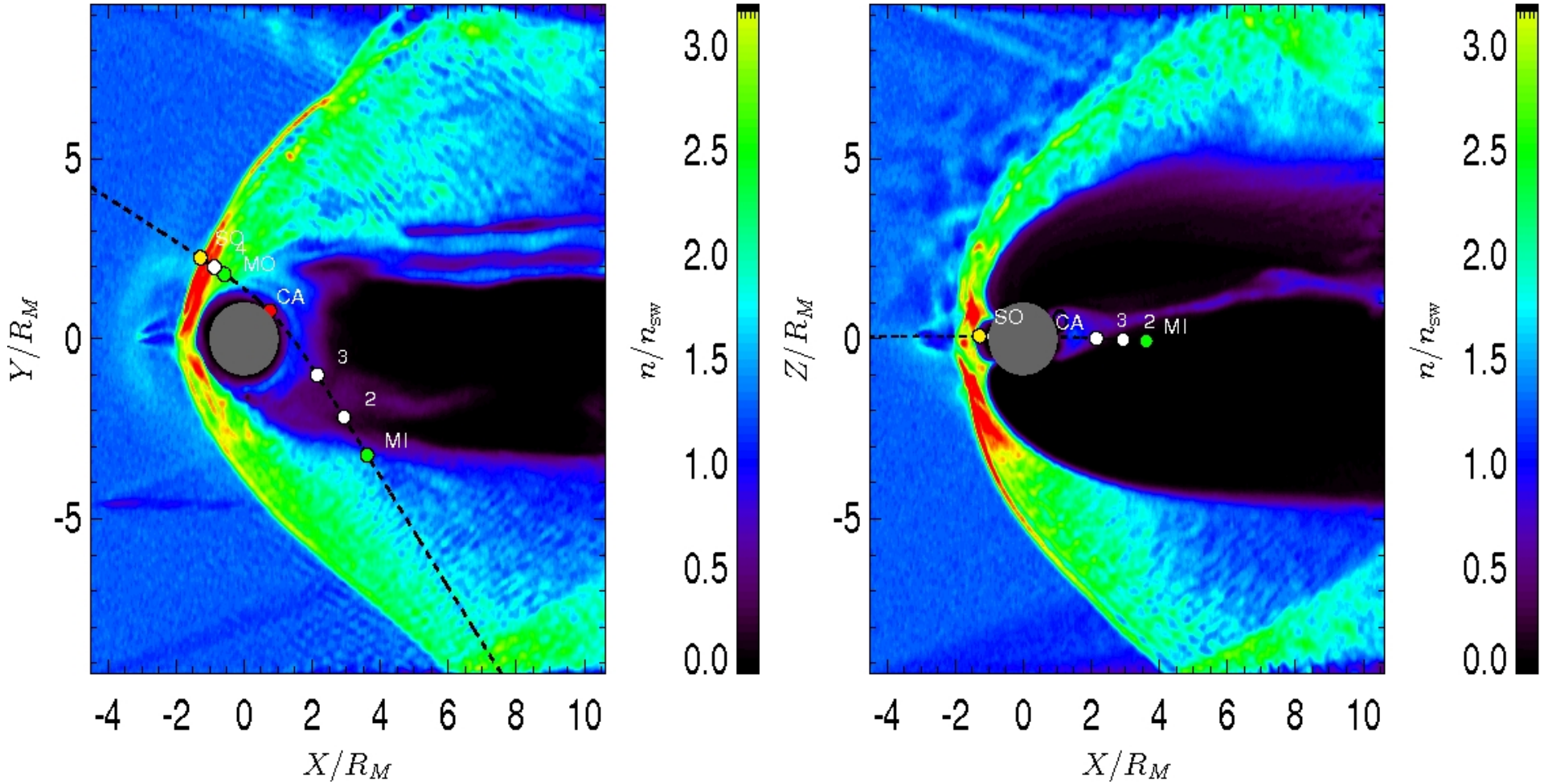

Flyby 2 (south-ward IMF): Simulated n_p/n_{psw}

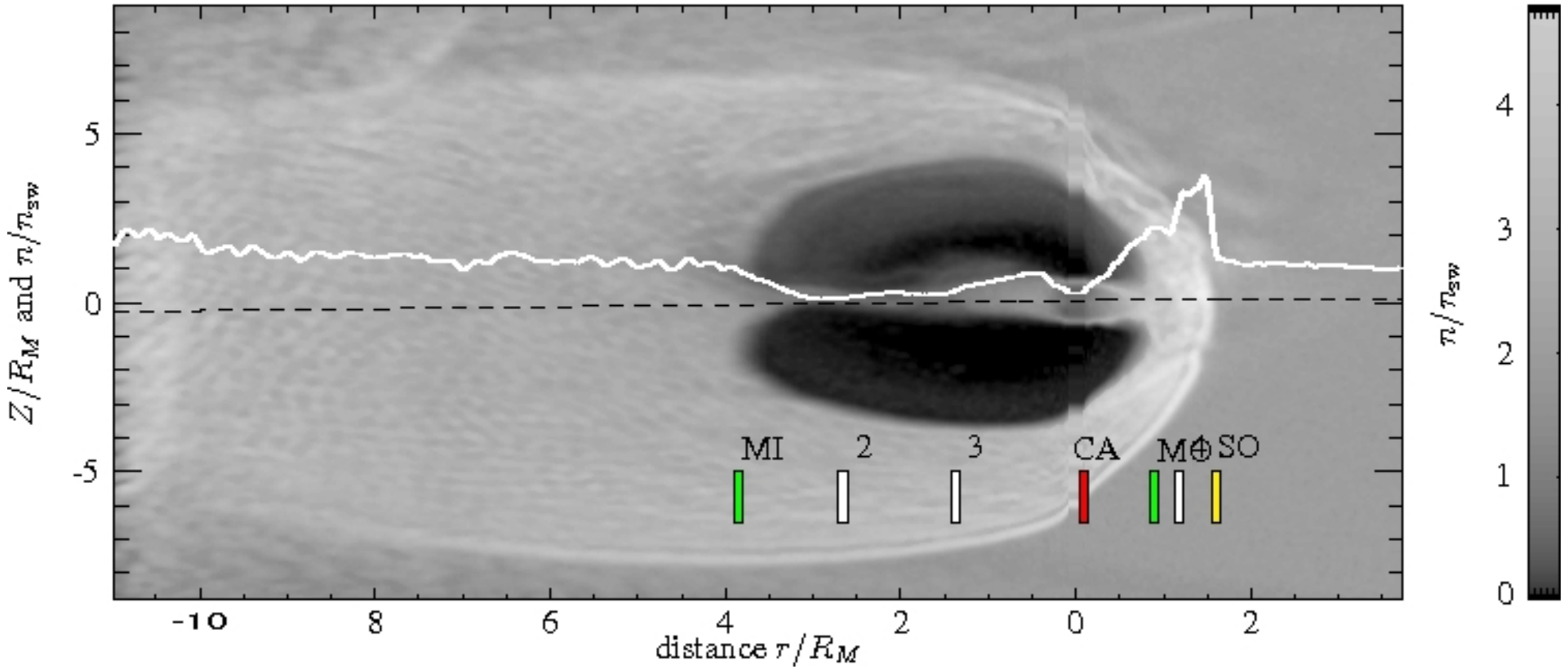

Flyby 2 (south-ward IMF): Simulated B/B_{sw}

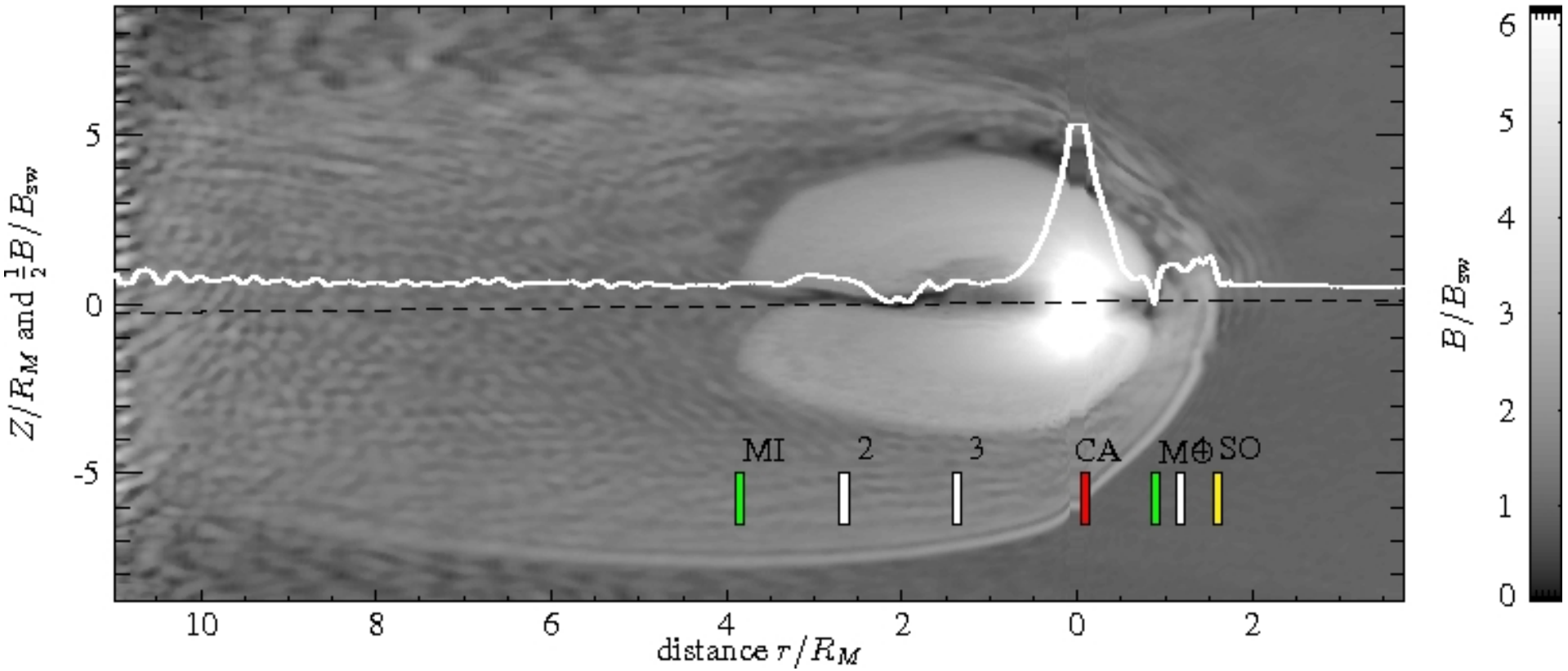

Flyby 2 (south-ward IMF): virtual and *in situ* measurements

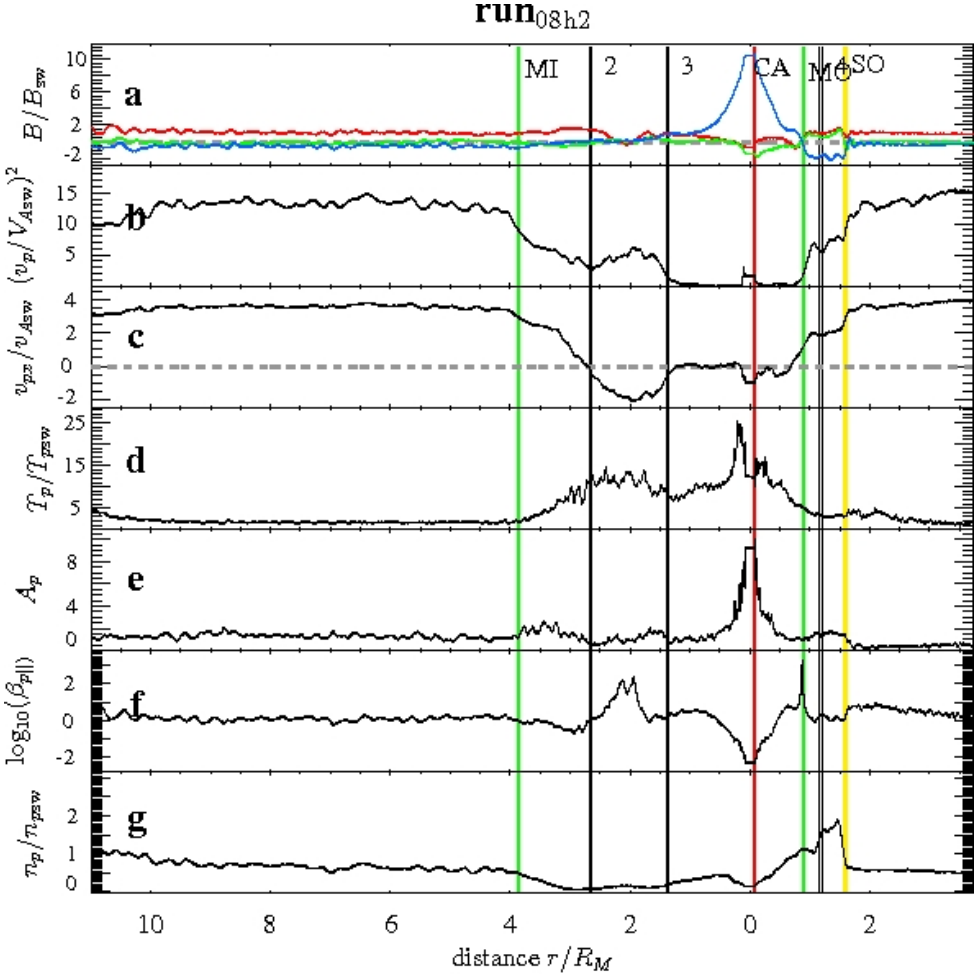

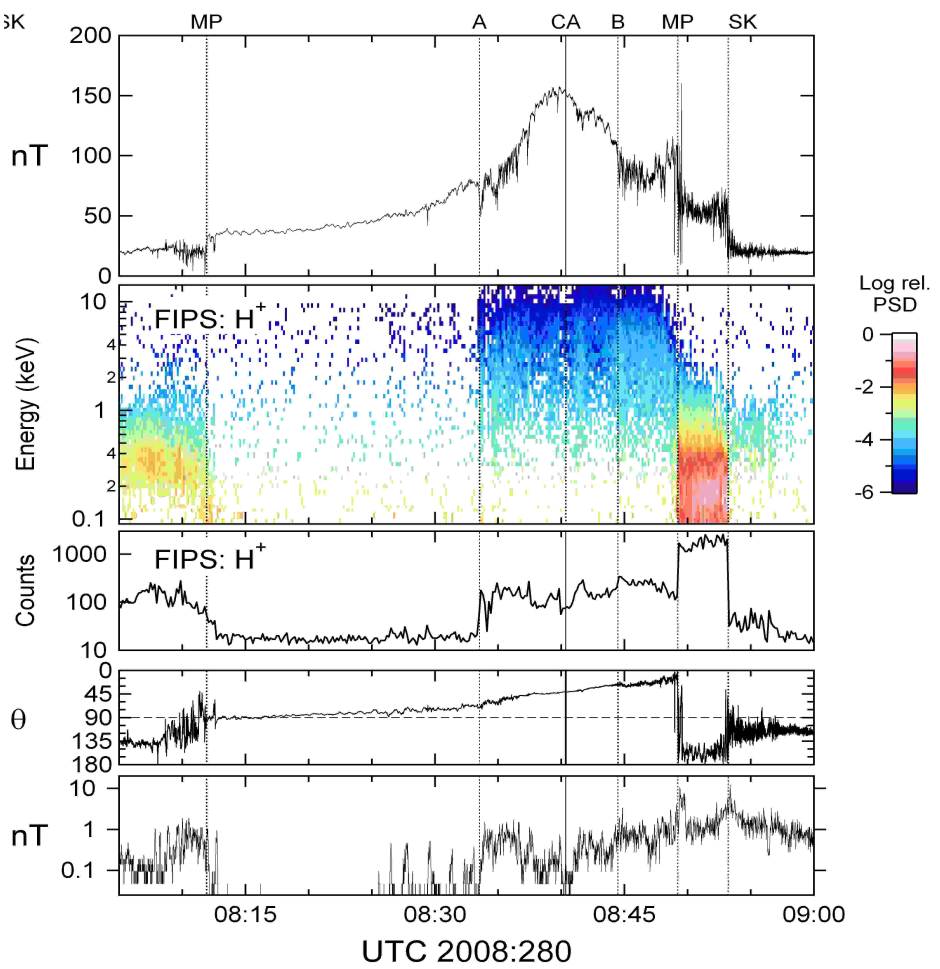

LEFT: virtual observations

RIGHT: MAG and FIPS *in situ* observations

Flyby 2 (south-ward IMF): S/C trajectory in $(\beta_{p\|}, T_{p\perp}/T_{p\|})$ space

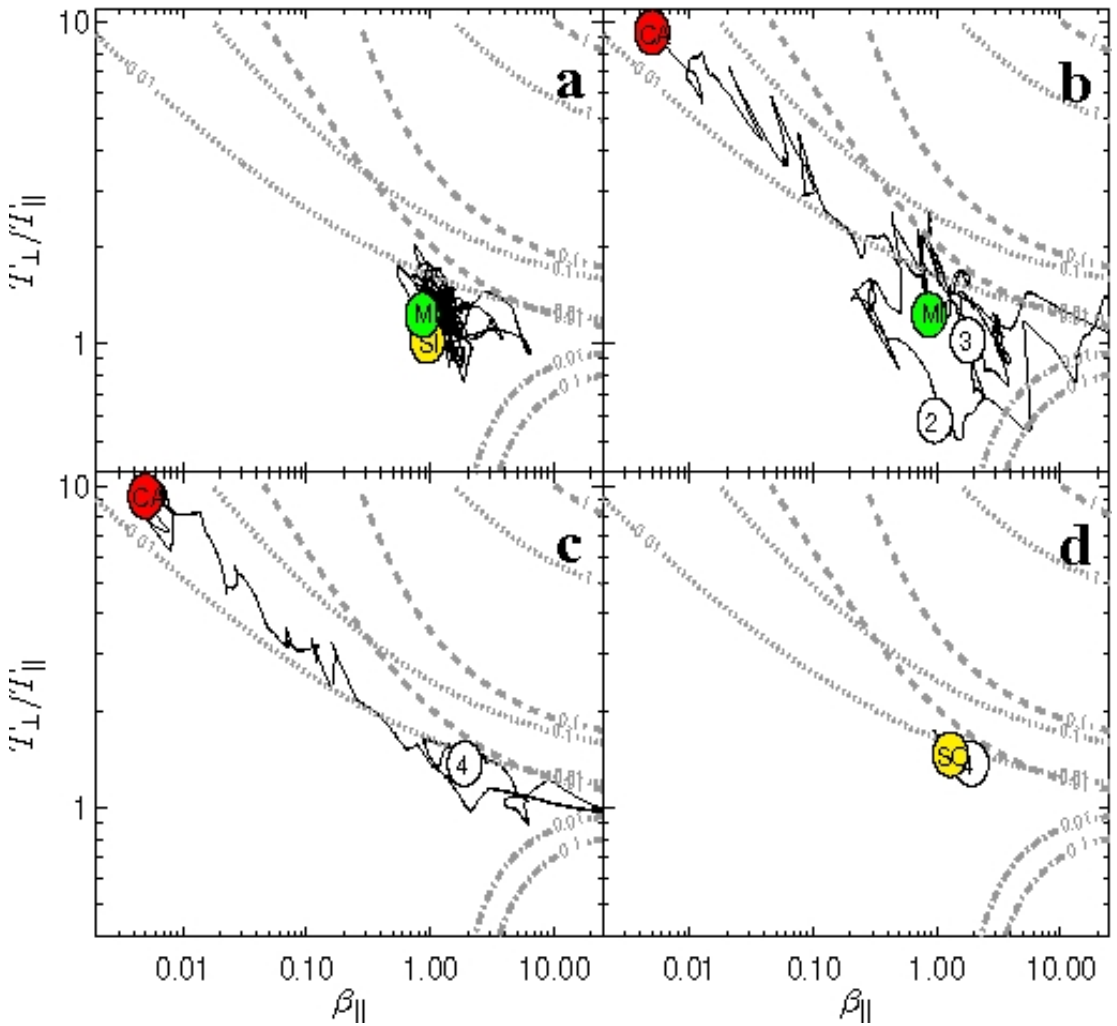

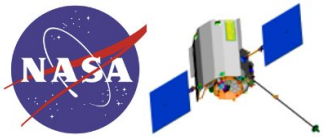

MESSENGER
Conclusions

- Both IMF configurations lead to a quasi-trapped plasma belt around the planet which may account for the diagmagnetic decreases observed on the inbound passes, as well as the ”double” magnetopause observed on the outbound leg of both MESSENGER flybys.
- For northward IMF, velocity shear leads to Kelvin-Helmholtz vortex type structures in the magnetopause, consistent with the first MESSENGER flyby observations on the inbound leg.
- For southward IMF, reconnection leads to plasmoid-like structures in the magnetotail, consistent with the second MESSENGER flyby observations in Mercury’s magnetotail
- An equatorial component of the IMF (i.e., By) is needed in order for the foreshock to form in the equatorial plane (from hybrid simulation results with IMF By not shown here); a foreshock was observed clearly during the first MESSENGER flyby, implying an IMF By at least some of the time.